# Evaluating the Application of a Shelf-Ready Reconstitutable Liquid Skin Substitute for Treatment of Full-Thickness Wounds in a Porcine Model

by

Amir Pourghadiri

B.Sc., The University of British Columbia, 2016

A THESIS SUBMITTED IN PARTIAL FULFILLMENT OF

THE REQUIREMENTS FOR THE DEGREE OF

MASTER OF SCIENCE

in

THE FACULTY OF GRADUATE AND POSTDOCTORAL STUDIES

(Experimental Medicine)

THE UNIVERSITY OF BRITISH COLUMBIA

(Vancouver)

July 2018

The following individuals certify that they have read, and recommend to the Faculty of Graduate and Postdoctoral Studies for acceptance, the dissertation entitled:

Evaluating the Application of a Shelf-Ready Reconstitutable Liquid Skin Substitute for Treatment of Full-Thickness Wounds in a Porcine Model

---

submitted by Amir Pourghadiri in partial fulfillment of the requirements for the degree of Master of Science

in Experimental Medicine

**Examining Committee:**

Dr. Aziz Ghahary
Supervisor

Dr. Reza Jalili
Supervisory Committee Member

Dr. David Granville
Additional Examiner

**Additional Supervisory Committee Members:**

Dr. Anthony Papp
Supervisory Committee Member

Supervisory Committee Member

## Abstract

Burn injuries affect millions of people worldwide, and can be one of the most difficult types of injuries to manage. Full-thickness burn wounds require immediate coverage, and the primary clinical approaches comprise of skin allografts and autografts. The use of allografts is often temporary due to the antigenicity of allografts. On the other hand, the availability of skin autografts may be limited in large burn injuries. In such cases, skin autografts can be expanded through the use of a skin mesher, creating the split-thickness meshed skin grafts (MSGs). Meshed skin grafts have revolutionized the treatment of large full-thickness burn injuries since the 1960s. However, contractures and poor aesthetic outcomes remain a problem. Skin substitutes can be employed as an alternative wound coverage for large full-thickness wounds, but most commercialized skin substitutes come in a pre-formed sheet, creating complications associated with tissue integration.

We previously fabricated an *in-situ* forming skin substitute, called MeshFill (MF), which can conform to complex shapes and contours of wounds. In this thesis, we hypothesized that the application of MF accelerated wound healing and improved aesthetic outcomes of fishnet-like scarring in MSGs. To test this hypothesis, the following objectives were employed: (1) assessing the wound healing outcomes of MF and (2) a combination of MF and MSGs in full-thickness excisional wounds in a porcine model. The results demonstrated that MF-treated wounds resisted contraction 20 days post-surgery, and the combination of MSGs and MF improved the aesthetic outcomes and reduced contractures examined through blinded evaluations. The results of this

pilot study provide a glance at MF's potential in improving the aesthetic outcomes of full-thickness wounds.

## Lay Summary

The gold-standard treatment for large burn injuries is the use of fishnet-like skin pieces, called meshed skin grafts. Although meshed skin grafts have saved patients' lives, they remain vulnerable to being contracted and forming undesirable scars.

We previously synthesized a liquid scaffold, called MeshFill, which can form a gel when added to the wound. Further, MeshFill emulates key aspects of the skin matrix. In this study, we examined the application of this gel in a pig wound model. This was accomplished by adding MeshFill in combination with the routinely used meshed skin graft or adding MeshFill alone to wounds.

In this animal model, we showed that MeshFill alone can resist contractions, and when combined with meshed skin grafts, the aesthetic outcomes of wounds were improved. We believe that this pilot study can provide insight into the potential applications of this gel in reducing scars seen in patients suffering from burn injuries.

## Preface

The research described in this thesis was conducted under the supervision of the Primary Investigator, Dr. Aziz Ghahary. Financial support was provided by WorkSafe BC, the BC Professional Firefighters' Burn Fund, and VGH & UBC Hospital Foundation.

Dr. Ghahary is also the leading investigator for a PCT patent for the powdered reconstitutable liquid scaffold, called MeshFill.

Chapters 2 and 3 are based on work conducted at BC Professional Firefighters' Burn and Wound Healing Research Laboratory. I was responsible for running experiments and analyzing the majority of the data presented in this thesis, and this was critically reviewed and approved by Dr. Ghahary. The surgeries and graft harvesting was conducted by Dr. Anthony Papp.

All methods and procedures, in addition to the use of animals and tissue specimens obtained from animals and humans, are approved by both Human and Animal Ethics Committee of the University of British Columbia (protocol numbers: H05-0103, A12-0296).

## Table of Contents

## List of Figures

## List of Abbreviations

Alpha-smooth muscle actin ($\alpha$-SMA)

Alternatively activated macrophages (M2)

Antibody (Ab)

Avidin biotin complex (ABC)

Chemokine ligand 17 (CCL-17)

Chemokine ligand 18 (CCL-18)

Classically activated macrophages (M1)

Cluster differentiation 3

Cluster differentiation 31 (CD31)

Damage-associated molecular patterns (DAMP)

Diaminobenzidine (DAB)

Dulbecco's modified eagle medium (DMEM)

Epidermal growth factor (EGF)

Extracellular matrix (ECM)

Fibroblast growth factor (FGF)

Full-thickness skin grafts (FTSG)

Glycosaminoglycan (GAG)

Hematoxylin and Eosin (H&E)

High-power field (HPF)

Interferon-$\gamma$ (IFN-$\gamma$)

Interleukin 1 (IL-1)

Interleukin 6 (IL-6)

Interleukin 10 (IL-12)

Interleukin 12 (IL-12)

Matrix metalloproteinases (MMPs)

MeshFill (MF)

Meshed skin (MS)

Meshed skin grafts (MSGs)

Meshed skin combined with MeshFill (MS+MF)

Natural killer cells (NK)

No treatment (NT)

Pathogen-associated molecular patterns (PAMP)

Phosphate buffered saline (PBS)

Platelet derived growth factor (PDGF)

Polyethylene glycol (PEG)

Polyvinyl alcohol (PVA)

Revolutions per minute (RPM)

Split-thickness skin grafts (STSG)

Standard error of the mean (SEM)

Subcutaneous (SQ)

Transforming growth factor ß1 (TGF-ß1)

Tris-buffered saline (TBS)

Tris-buffered saline containing Triton-X 100 (TBS-T)

Tumor necrosis factor-$\alpha$ (TNF-$\alpha$)

United states (US)

Vascular endothelial growth factor (VEGF)

## Acknowledgements

I would like to express my sincere gratitude to my supervisor, Dr. Aziz Ghahary, for providing me with this learning opportunity. The guidance, motivation, and immense knowledge you have provided has helped me become a better and more creative scientist.

I would also like to thank my parents, brothers, and friends who have provided unequivocal support this journey. Thank you for keeping a positive attitude and instilling in me the work ethic and optimism I adopted throughout graduate school.

A sincere thanks to my committee members, Dr. Reza Jalili and Dr. Anthony Papp for their guidance and mentorship through this process.

I am extremely thankful for my laboratory colleagues, Dr. Ruhi Kilani, Dr. Layla Nabai, Dr. Yunyuan Li, Dr. Hatem Nojeidi, and Dr. Ali Farrokhi, who have provided me with technical and intellectual knowledge that I will carry as I continue my career.

**Dedication**

I dedicate this thesis to my parents who have sacrificed so much for me to continue my journey while providing endless support throughout my life.

## Chapter 1: Introduction

### 1.1 Skin physiology and wound healing

Skin is the largest organ in the body and provides a protective barrier against pathogens and ultraviolet light (1). Skin can be divided into two sections: the epidermis and dermis. The epidermis is a non-vascularized stratified epithelium undergoing continuous renewal through mitotically active basal layer keratinocytes (2). The stratum basale sends finger-like projections towards the dermis, forming an undulating appearance called rete ridges. The thickest layer, stratum spinosum, contains tetrahedral keratinocytes with limited mitotic activity. The stratum granulosom is where keratinocytes flatten and produce keratohyalin granules. Few anatomical regions, such as the palms of the hand and soles of the feet, have a transparent stratum lucidum layer expressing eleidin, an intermediate product of keratin synthesis. Finally, the outermost layer, stratum corneum, contains enucleated and interlocking corneocytes, and functions to prevent water loss (3). Keratinocytes make up approximately 90% of cells in the epidermis, and the remaining 10% include Langerhans cells, melanocytes, and Merkel cells (2).

Unlike the epidermis, the dermis is a supporting matrix with rich vasculature (4). Additionally, dermis is a tough elastic tissue due to the expression of collagen and elastin. Collagen and elastin comprises 80-85% and 2-4% dry weight of the dermis, respectively (5, 6). There are over 29 types of collagens identified; however, type I and III collagen fibers make up the majority of the dermis (7). Other components of the dermis include glycoproteins such as fibronectins, fibulins, and integrins, which allow for

cell adhesion and mobility (2). A family of proteins maintaining hydration of the dermis are proteoglycans, which make up 0.1-0.3% of the dermis (8).

When an insult damages the epidermis and dermis, an ordered and timely repair process begins in acute wounds to regain structural integrity and function. The mammalian response to an insult consists of hemostasis, followed by three overlapping phases: inflammation, proliferation, and tissue remodeling (figure 1.1) (9, 10). These phases are coordinated by a myriad of signals and interactions from soluble mediators, cells such as platelets, fibroblasts, keratinocytes, in addition to endothelial and immune cells.

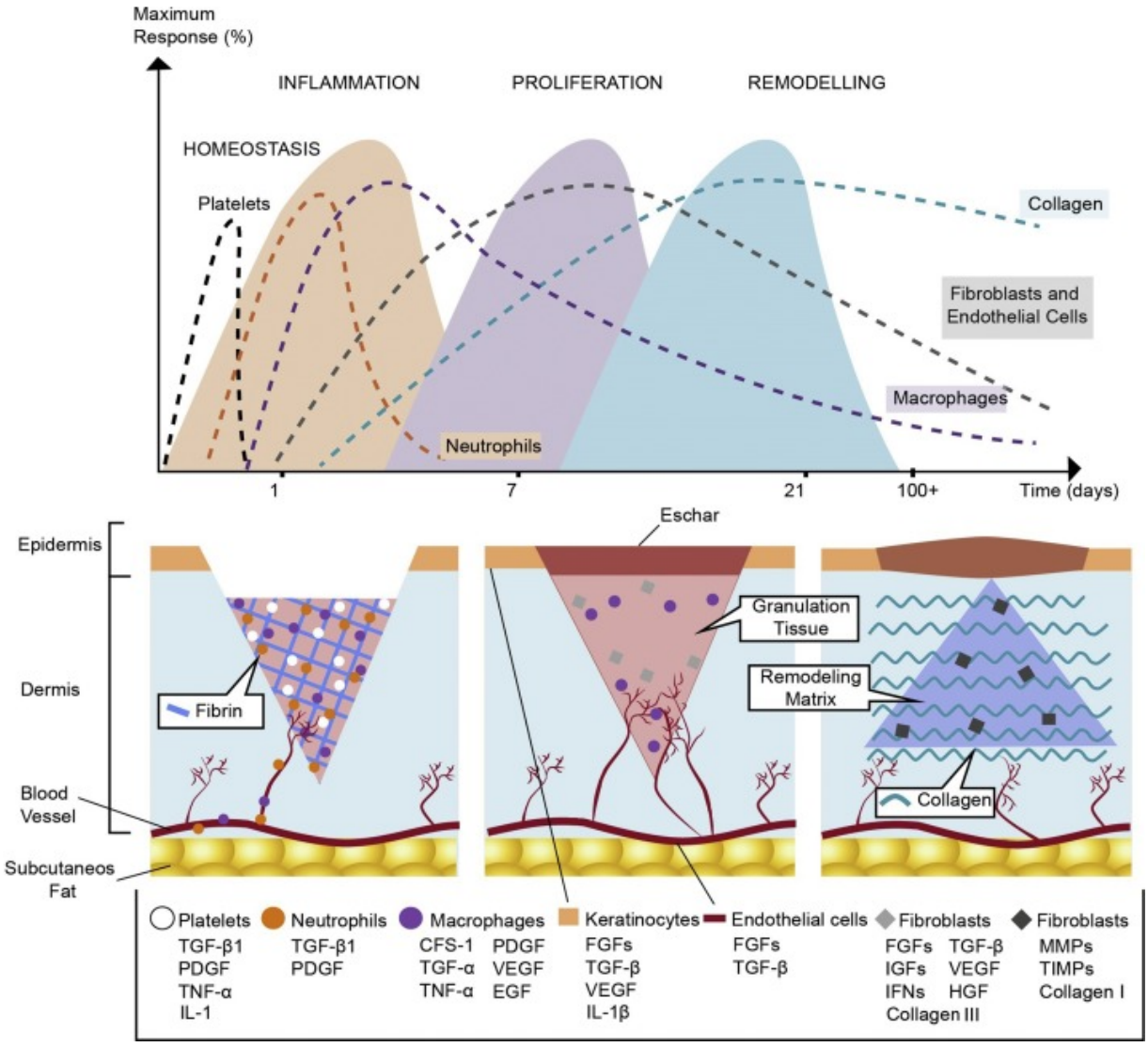


**Figure 1.1. Wound healing phases.** The upper and lower panel show the types of cells and extracellular matrix molecules involved in the three wound healing phases. Figure adopted from Zomer, Tretin, Journal of Dermatological Science, 2018. Permission obtained (10).

Upon an insult, blood vessels undergo trauma, leading to vasoconstriction and recruitment of platelets to form a platelet plug, followed by formation of a provisional

fibrin matrix that plays a pivotal role in cell adhesion, migration, and beginning tissue repair (1, 11).

In the first 24 hours, platelets secrete platelet derived growth factors (PDGF), which acts as a chemotactic agent to attract neutrophils, macrophages, and fibroblasts to the wound site (12). Neutrophils are one of the first cell types in the inflammatory phase, and function to clean out debris and invading pathogens. However, through the action of elastases, neutrophils presence over time can degrade extracellular matrix (ECM) in addition to clotting factors, cytokines, and immunoglobulins (13). Thus, neutrophils withdrawal in an appropriate and time-sensitive manner is an essential component to the advancement of wound healing (14). Macrophages are the key players involved in removal of neutrophils; upon injury to the skin, resident and circulating monocytes are exposed to two types of signals: damage-associated molecular patterns (DAMP) and pathogen-associated molecular patterns (PAMP). DAMP includes molecules such as DNA, RNA and intracellular proteins expressed by necrotic cells. On the other hand, PAMP are foreign molecules expressed by pathogens, such as polysaccharides and polynucleotides. In combination, PAMP, DAMP, interferon-$\gamma$ (IFN-$\gamma$) derived from natural killer (NK) cells drive differentiation of monocytes to classically activated macrophages (M1) (15). In turn, M1 macrophages produce pro-inflammatory mediators, including interleukins 1,6, and 12 (IL-1, IL-6, IL-12), tumor necrosis factor-$\alpha$ (TNF-$\alpha$), and chemokines to further recruit leukocytes (16-18). Moreover, M1 macrophages phagocytose microbes and cellular debris, in addition to apoptotic neutrophils, in a process called efferocytosis (1, 9, 19). As the inflammatory phase subsides, macrophages transition to a reparative M2 phenotype, expressing anti-

inflammatory cytokines (IL-10, IL1-receptor antagonist), chemokine ligands 17 and 18 (CCL-17, CCL-18) and growth factors, such as transforming growth factor ß1 (TGF-ß1), PDGF, vascular endothelial growth factor (VEGF), and epidermal growth factor (EGF) to promote fibroblast proliferation, ECM production, and angiogenesis (18, 20).

Transitioning to the proliferative phase shifts priorities towards granulation tissue formation, angiogenesis, and re-epithelialization (1). The provisional matrix formed upon an insult provides a channel for cell migration, aiding the formation of granulation tissue by allowing fibroblasts to bind to fibrin and secrete collagenous matrices (21). Angiogenesis involves complex interactions of soluble factors acting in an orchestrated fashion (22). Endothelial cells lining the blood vessels are exposed to the hypoxic environment of the wound, in addition to vascular endothelial growth factor (VEGF), angiopoietins, fibroblast growth factor (FGF), becoming activated. (23-26) Activated endothelial cells release proteolytic enzymes, detaching from their basement membrane, and migrating into the wound bed. Matrix metalloproteinases (MMPs) continue to break down the surrounding matrix as vessels are formed, and pericytes release inhibitory factors to stabilize endothelial cells (27, 28). Re-epithelialization is established by dissolving cell-cell contact through interrupting hemi-desmosomes and desmosome connection to allow keratinocytes to migrate from the wound edge, where they begin to cover the un-epithelialized layer (29, 30). Once this gap is closed, cell-cell contact is established and keratinocytes begin building the basement membrane (30). To facilitate wound closure and deposit ECM, myofibroblasts appear in proliferative phase, expressing alpha-smooth muscle actin ($\alpha$-SMA) (31).

The remodeling phase begins approximately two weeks after injury, and can last for more than one year (11). In this phase, the ECM composition and alignment changes in attempt to regain structural integrity. However, healed wounds are only able to regain 80% of the tensile strength of healthy skin (32). Granulation tissue, rich in type III collagen and blood vessels, begins to degrade through the action of matrix metalloproteinases (MMPs), mediated by endothelial cells, fibroblasts, and macrophages, while being replaced with type I collagen (9, 33, 34). Though healthy skin is composed of approximately 90% type I and 10% type III collagen, granulation tissue undergoes a transient increase in type III collagen (40%) before these levels begin to normalize during the late remodeling phase of wound healing (35, 36). In general, type I collagen is thicker in diameter and recognized for its high tensile strength and torsional rigidity, whereas type III collagen is thinner and has reduced mechanical stiffness (37, 38).

During the remodeling phase, cellularity decreases through apoptosis of myofibroblasts and vascular cells (39, 40). This phase requires the correct balance of ECM synthesis, degradation, and apoptosis to ensure successful wound healing. Pathological anomalies in this process can lead to excess fibrosis and hypertrophic scarring (1).

### 1.2 Skin grafts

According to the World Health Organization, more than 300,000 people die from fire-related burn injuries annually (41). Of paramount importance to treating deep dermal injuries is wound closure. However, often times, even when wound closure is

attained, it can come at the expense of aesthetic and functional impairments (42-44). Burn injuries can be one of the most difficult types of insults to manage, as fluid loss and tissue damage, combined with wound infection and potential systemic immune response can lead to sepsis and organ failure (45, 46).

Currently, the gold standard of treatment for deep burn injuries are skin grafts, which are defined as cutaneous tissue taken from a donor site and transplanted onto a recipient site. Skin grafts can be divided into two general categories: full-thickness skin grafts (FTSG) and split-thickness skin grafts (STSG). Full-thickness skin grafts contain the epidermis and entire dermis, while STSG contain the epidermis and varying thicknesses of the dermis. Within each category, there are a number of different types of grafts.

The use of skin grafts originated around 3000 years ago in India (47, 48). Over time, there were only few reports for their application until 1869 when the technique was rediscovered and revamped by Reverdins advent of pinch grafts (49). Using a scalpel, Reverdin pinched and excised a piece of skin that was subsequently transplanted on a patient with limb loss. These islets of skin grafts were reported to accelerate healing, but the problem of contracture remained. The turning point of skin grafts was between when Leopold Ollier and Carl Thiersch invented the dermoepidermal grafting technique, known today as split-thickness skin grafts, using a razor to control the thickness of the dermis. Ollier-Thiersch protocol proposed the excision of granulation tissue before placing the graft on the wound bed. Between 1875-1893, application of FTSGs were indicated in various medical specialties, including ophthalmology, neurosurgery, and plastic surgery. From 1914-1950s, instrumental and technical refinements, such as

instruments with improved control of dermal thickness and mechanical dermatomes, were introduced to facilitate the process of skin grafting. In 1964, Tanner and Vandeput revolutionized treatments for burn and reconstructive surgeries by introducing meshed skin graft (discussed in section 1.2.2) to cover large wounds (50).

Each type of skin graft has benefits and limitations, and their applications vary depending on the site and size of the wound. Split-thickness skin grafts can thrive with less recipient wound bed vascularity due to lower metabolic demands, but are more likely to undergo a greater overall contracture (51, 52). Further, STSG are more susceptible to trauma and may pigment abnormally (peripheral hypopigmentation and graft hyperpigmentation) (53-55). In contrast, FTSG require a rich vascularized wound bed, not only due to nutritional requirements, but also to promote a collagenous matrix that adheres to recipient wound bed (55).

### 1.2.1 Healing stages of autologous skin grafts

When skin grafts are transplanted onto the wound bed, the ‘take’ of the graft is not guaranteed. Once transplanted, a thin layer of fibrin attaches the graft to recipient site. However, the harvested graft undergoes a period of ischemia. In the first 24-48 hours, imbibition prevents the desiccation of skin through passive diffusion of serum (56). In this process, the graft becomes edematous and can gain as much as 37% of its initial weight (55, 56). This is proposed to be mediated by extracellular molecules, such as proteoglycans, which absorb water and ions from the wound bed (57). The purpose of this process is thought to allow for graft survival before vascularization is established.

An evolving discussion in the literature is the mechanism by which vascularization occurs between the recipient wound bed and skin graft. Over approximately 50 years, two theories have been put forward; One is inosculation, or the direct connection of severed vessels from skin graft vasculature to host wound bed (58-65). Another theory is neovascularization, or *de novo* angiogenic ingrowth of vessels from the wound bed into the graft (66-70). Although there has not been a clear consensus in more than half a century, recent studies utilizing new genetic techniques have begun to elucidate the mechanism of vascularization. In one study using transgenic *tie2*/*lacZ* mice as recipient and FVB/N (control) mice as skin graft donor, the authors were able to show vascular ingrowth occurs from the periphery of the skin graft towards the center from day 3 to 21, with inosculation occurring at day 7 (71). In a reciprocal model using *tie2/lacZ* mice as donor and FVB/N mice as recipient, the authors showed donor vessel regression occurred as early as day 3, and complete regression of peripheral vessels by day 7. However, the central portion of the graft vessels remained intact until the terminal point of the study (day 21). In contrast, another study published the same year using fluorescein isothiocyanate (FITC) showed vessel anastomoses at the center of the graft after 2 days (72). Based on studies in the past 50 years, and the *ex-vivo* studies described, it is probable that a combination of both theories are part of this process. Future studies utilizing *in-vivo* visualization of blood vessels will provide insight into the mechanisms underlying skin graft vascularization (73).

### 1.2.2 Meshed skin grafts

Split-thickness meshed skin grafts (MSGs) are the gold-standard for treatment of large burn injuries (74). The meshed skin graft (MSG) was first described by Tanner and Vandeput in 1964 as a method to expand skin grafts, and has been utilized as the standard of care to date (75). Surgeons utilize special meshing devices to achieve expansion ratios of 1:1, 1.5:1, 2:1, 3:1, 4:1, 6:1, and 9:1 (76, 77). The length of void areas in MSGs is directly related to these expansion ratios (78).

The use of MSGs allows one to use a smaller donor area per given recipient wound area. Further, MSGs take well and conform to complex and uneven surfaces, in addition to providing void areas for serum or exudate drainage, thereby ensuring better graft take and increasing resistance to infection (50, 76). Granulation tissue developing at fenestrated sites, in combination with tie-over dressing, help immobilize the graft (79). However, fenestrated sites heal by secondary intention, leading to a fishnet-like scar formation and aesthetically undesirable outcomes (76, 80). Despite the drawbacks, MSGs remain the current standard of care due to their ease of use and efficacy in treating large burn injuries.

## 1.3 Experimental animal models of wound healing

### 1.3.1 Mouse as an animal model

The primary goal of research animal models is to attempt to create conditions emulating the complexity of wound healing. Thus, an animal model capturing the physiology and pathology underlying human wound healing is essential (10). To date, mice represents the most popular animal model to examine wound healing outcomes

for several reasons. Mice have been historically utilized to elucidate disease pathology; as a result, mice models can provide effective ways to minimize differences and confounding variables by matching the age, weight, sex, and genetic differences in a study (10). In addition, mice are easy to handle, reproduce rapidly, and provide a cost-effective framework to increase the number of replicates, thereby improving power and statistical validation of studies (10, 81). Finally, antibodies and transgenic mice are readily available, facilitating the expenditure of time and finances for a given study (82).

Despite the advantages of mice models in wound healing, there are key interspecies differences which lead to challenges when attempting to bridge the gaps between human and mice. First, due to the presence of a thin intradermal muscle layer, panniculus carnosus, and relatively weak adherence of the dermis to the subcutaneous tissue, mice wounds heal by contraction (82, 83). The second notable difference is the dense hair coat mice adopt, which allows for faster epithelialization of wounds since the hair follicles surrounding the wound can aid in the process of epithelialization.

Due to the wide use of mice in wound healing research, Gerber et al. (2014) set out a study to compare the expression of human and mouse transcriptomes using the genome wide database (84). After generating a list of human skin-specific genes and comparing them to mouse, the authors found a total of only 30.2% identity between the two species. Most of the shared genes encoded structural and barrier proteins, such as genes related to keratin family, and cell-cell junction.

Although mice appear to provide a great model for wound healing due to the availability of tools and ease of use, their translational potential has been limited in providing effective therapies for treating various types of wounds (10). Comparatively,

rats represent the second most popular animal model used in recent wound healing studies (82). However, due to the similarities in wound healing physiology of rodent models, mice are generally preferred. Further, mutant mice models are more readily available compared to rat models.

### 1.3.2 Porcine as a model of wound healing

Pig and human skin are similar in many aspects with regards to skin physiology and wound healing. First, when compared to humans, pigs show a similar epidermal thickness and turnover, in addition to distribution of blood vessels in the dermis and expression of keratinous proteins (82). Further, one of the most important distinctions between pig and mouse models of healing is that pig wound healing occurs primarily through epithelialization than contraction. Pigs also reveal an alarming 78% concordance with human studies, whereas mice only show a 53% concordance (85).

However, the use of pigs as an animal model does come with challenges as pigs require training, a dedicated vivarium and staff, and the availabilities of antibodies and growth factors are limited (86). Further, economic constraints due to limited funding has led to slower progress and lower priority placed on using translatable animal models in basic research (82). Thus, despite the advantages of pig models, the majority of publications since the 1960s have utilized rodent models to examine wound healing (figure 1.2 A). Further, limited funding, combined with increasing costs associated large animal care has added to the lower use of pig models in wound healing research (figure 1.2 A,B)

As explained above, animal models can make a major impact on the results and progress of translational research. Studies using mice as an animal model have led to invaluable data, providing insights into mechanisms and pathophysiology involved in wound healing. However, the pitfalls and limitations of one animal model can be compensated for by utilizing a more suitable and representative animal model, such as pigs. Doing so can lead to faster transition of studies from bench to bedside, and ultimately better patient care.

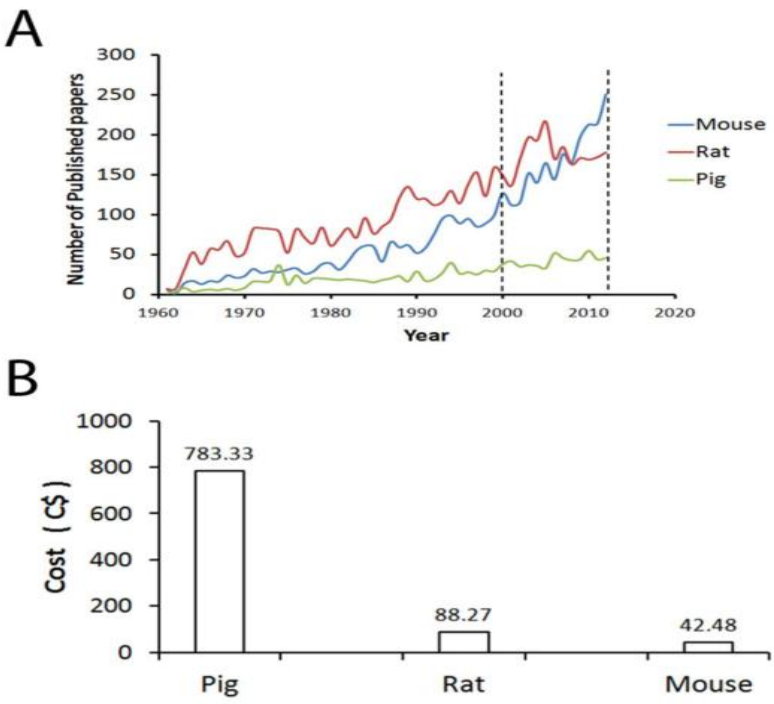


**Figure 1.2**. **Trends and costs associated with animals in burn research.** Publications and costs associated with animals in wound healing research. **A:** Number of publications for each species in the PubMed database since the 1960s. **B:** The cost (in Canadian dollars) associated with housing, delivery and purchase of each species for 30 days. Figure adopted from Abdullahi, Amini-Nik, Jeschke, Cellular and Molecular Life Sciences, 2014. Permission obtained (82).

### 1.4 Skin substitutes in wound healing

The wound healing timeline is contingent on the extent of dermal injury. Prompt care in burn injuries are crucial, not only to prevent wounds from infection, drying, and increasing in severity, but also to minimize scar appearance once wounds have healed (87). Unfortunately, deep dermal injuries covering a large portion of the body often result in scar tissue and deformities, and correctional surgeries are confined in achieving optimal aesthetic outcomes. Thus, upon insult, the ideal situation is to induce skin regeneration promptly.

Skin substitutes have attempted to fulfill this role; however, products in the market, such as human cadaveric allografts, semi-synthetic (Biobrane®), and bioengineered membranes (TransCyte®) can be either expensive, allogenic, vary in quality, difficult to obtain, or a combination of the above factors (77, 88). Further, most skin substitutes available in the market are pre-formed constructs, which can limit their application in complex wounds containing irregular surfaces.

Thus, an ideal skin substitute should adopt clinically feasible and biocompatible characteristics. From a clinical standpoint, skin substitutes should be shelf-ready, easy to store, conform to complex shapes and pores of wounds, and maintain a moist environment in wounds (89). Further, biocompatibility will allow products to integrate well with surrounding tissue while minimizing antigenicity. Skin substitutes should also provide a temporary scaffold, with controlled degradation, to induce fibroblast infiltration, faster epithelialization, and promote collagen synthesis.

## 1.5 Previous findings

A major limitation in collagen skin substitute fabrication is the gelation temperature and time. Previously, our lab synthesized an *in-situ* forming hydrogel, called MeshFill (MF), by stabilizing cross-linked collagen:glycosaminoglycan (GAG) matrix with polyvinyl alcohol (PVA), polyethylene glycol (PEG), and borates (90). This mixture permitted lyophilisation of this mixture, reconstitution in distilled water, and subsequent gelation at a working range of 30 ºC- 37 ºC in approximately 15 minutes (90, 91). Further, this hydrogel adopted a significantly higher tensile strength when compared to crosslinked and uncrosslinked collagen:GAG matrices with/without borates (91). Indeed, as opposed to a gel-slurry, this hydrogel can be sutured, similar to pre-formed solid scaffolds (90). *In-vitro* studies of MF revealed its resistance to contraction when cultured with fibroblasts derived from healthy patients and patients with hypertrophic scars (92). In addition, while high cellularity and contraction is associated with tissue fibrosis, MF reduced cell proliferation and contraction without compromising the viability of primary fibroblasts and keratinocytes. By applying MF to a rabbit ear wound healing model, our group also showed improved wound healing outcomes on multiple factors. Clinically, the application of MF reduced scar elevation index. However, immunofluorescence results showed reduced T-lymphocyte infiltration, better cutaneous vascular perfusion and innervation of the dermis.

## 1.6 Hypotheses and objectives

The goal of this master's thesis is to examine the wound healing outcomes of an *in-situ* collagen composite hydrogel in a porcine model. In our previous findings, we

reported that the application of MF resisted contraction *in-vitro,* while reducing cell proliferation, scar elevation index, cellularity, and improved vascular perfusion and innervation *in-vivo*. Transitioning towards a wound healing model that closely resembles human skin physiology, we used Yorkshire pigs to examine the application of MF in full-thickness wounds. As mentioned previously, void areas in MSGs heal by secondary intention, leading to contraction and ultimately a fishnet-like scar formation. Thus, we examined whether the addition of MF in void areas would permit better aesthetic outcomes of healing.

My overall hypothesis for this project is that the application of this hydrogel, named MeshFill (MF), improves healing outcomes of a full-thickness wound model in Yorkshire pigs.

**Objective 1**

Examine wound healing outcomes of MF in full-thickness excisional wounds. These parameters include epithelialization, contraction, histology, and immunohistochemistry experiments characterizing healing outcomes.

**Objective 2**

Assess the aesthetic and wound healing outcomes when combining MSGs and MF through blinded clinical evaluations, contracture analysis, histological and immunohistochemical staining.

## Chapter 2: Examining the application of an in-situ forming hydrogel in full-thickness excisional wounds in Yorkshire pigs

### 2.1 Introduction

Acute burns or large wounds may compromise skin function. In these cases, patients are in an immediate need of wound coverage to reduce their chances of infection, and promote regeneration and repair (93). Wound care is a large financial burden on healthcare, costing $25 billion dollars (USD) per annum in the United States (US) (94). It has been estimated that the average cost of a patient with burn injury is nearly $90,000 (USD) in high-income countries (95). Therefore, a demand for a clinically feasible product that would help patients regain functional tissue with an aesthetically desirable outcome is paramount.

To date, the most common clinical approach in covering full-thickness burn injuries is using allografts and autografts (96). Allografts are often utilized as temporary wound coverage as the host tissue elicits an immune response against foreign antigens of the graft (97). On the other hand, the use of autografts for treatment of large burn injuries can be challenging due to the limited availability of healthy donor sites.

To improve caveats existing in these grafts, various skin substitutes have been introduced in the field of tissue engineering. A skin substitute is a biological skin that serves to restore aspect(s) of skin function (fluid drainage, moisture, and epithelialization) (93). There are various types of skin substitutes in basic research, clinical trials, and even commercially available skin substitutes. These include epidermal and dermal analogs (Biobrane®, Integra®) and skin substitutes seeded with fibroblasts

or keratinocytes (Dermagraft®, Apligraft®, Orcel®, Epicel®, Stratagraft®) (96, 98). The problem with many of these products is that they are manufactured as pre-formed sheets, making them unsuitable for conforming to wounds with irregular surfaces and pores, thereby increasing the chances of complications associated with tissue integration (90). Other limitations in bioengineered scaffolds include reduced vascularization, poor mechanical integrity, and antigenicity (99). Therefore, these factors impede the use of some skin substitutes, increasing the demand for alternative therapeutics.

Tissue engineering innovations have led to the development of hydrogels to treat injuries of the skin, skeletal muscle, heart, bone, and spinal cord (100). Simply, hydrogels are cross-linked molecules that can absorb water without dissolving (101). As scaffold preparation is one of the core facets of tissue engineering, hydrogels should provide moisture while being malleable and exhibiting mechanical properties (strength, viscosity, elasticity). Polymers used in hydrogels can be derived from natural (collagen, fibrin, gelatin, alginate) or synthetic sources (polyglycolic acid, poly-ß-hydroxybutyrate, polycaprolactone) (102).

Collagen and its recombinant forms represent the most popular polymers used in hydrogels due to their cross-linking ability, mechanical strength, biocompatibility, and low antigenicity (102). For hydrogels to be clinically applicable in chronic wounds and burn injuries, an *in-situ* forming scaffold is preferred to ensure coverage of tunnelled areas or irregular surfaces present in the wound (90). Previously, we have shown that a freeze-dried polyvinyl alcohol (PVA)-polyethylene glycol (PEG)-collagen composite scaffold permitted gelation *in-situ* subsequent to reconstitution in water (90). Translating

this PVA-PEG-collagen hydrogel to an *in-vivo* rabbit ear model, our group has shown improved wound healing outcomes in scar elevation index, vascular perfusion, and cutaneous innervation (92). In order to transition towards a patient-ready *in-situ* forming hydrogel, we sought to assess the application of MeshFill (MF) in a full-thickness porcine model.

## 2.2 Methods

### 2.2.1 Cell culture and viability

MeshFill (MF) was synthesized as previously described (figure 2.1) (90, 92). Before conducting our animal model experiments, MF was examined for toxicity. Foreskin samples were obtained from healthy individuals undergoing elective circumcision, and fibroblasts were subsequently harvested as previously described (103). Fibroblasts (passages 3-5) with triplicates from three different donors were utilized for this experiment. After cultured fibroblasts were trypsinized, neutralized with dulbecco's modified eagle medium (DMEM), and centrifuged at 1400 revolutions per minute (RPM) for 5 minutes, 2.5 x $10^5$ fibroblasts were mixed with 200 µl of hydrogel after being reconstituted in distilled water. Cells suspended in hydrogels were subsequently transferred to a 48-well culture plates and incubated at 37ºC to allow gelation to occur (gelation time: 10-20 min). After wells were examined for complete gelation, 300 µl of DMEM supplemented with 10% fetal bovine serum and 1% antibiotic-antimycotic was added on top of each well.

Cell viability was assessed after 2, 4, 7, and 14 days using the Live/Dead® viability/cytotoxicity assay kit for mammalian cells. This assay utilizes ethidium

homodimer (EthD-1) and calcein AM to stain for dead cells and live cells in red and green respectively. In order to conduct this assay, gel-cell mixtures were washed three times with 1x phosphate buffered saline (PBS) solution. Subsequently, a mixture containing 2 μM calcein AM and 4 μM EthD-1 was added to each well, and incubated for 30 minutes at 37ºC. Cell viability was visualized using a Zeiss Axiovert 200M fluorescence microscope or Zeiss AxioObserver.Z1 inverted confocal microscope.

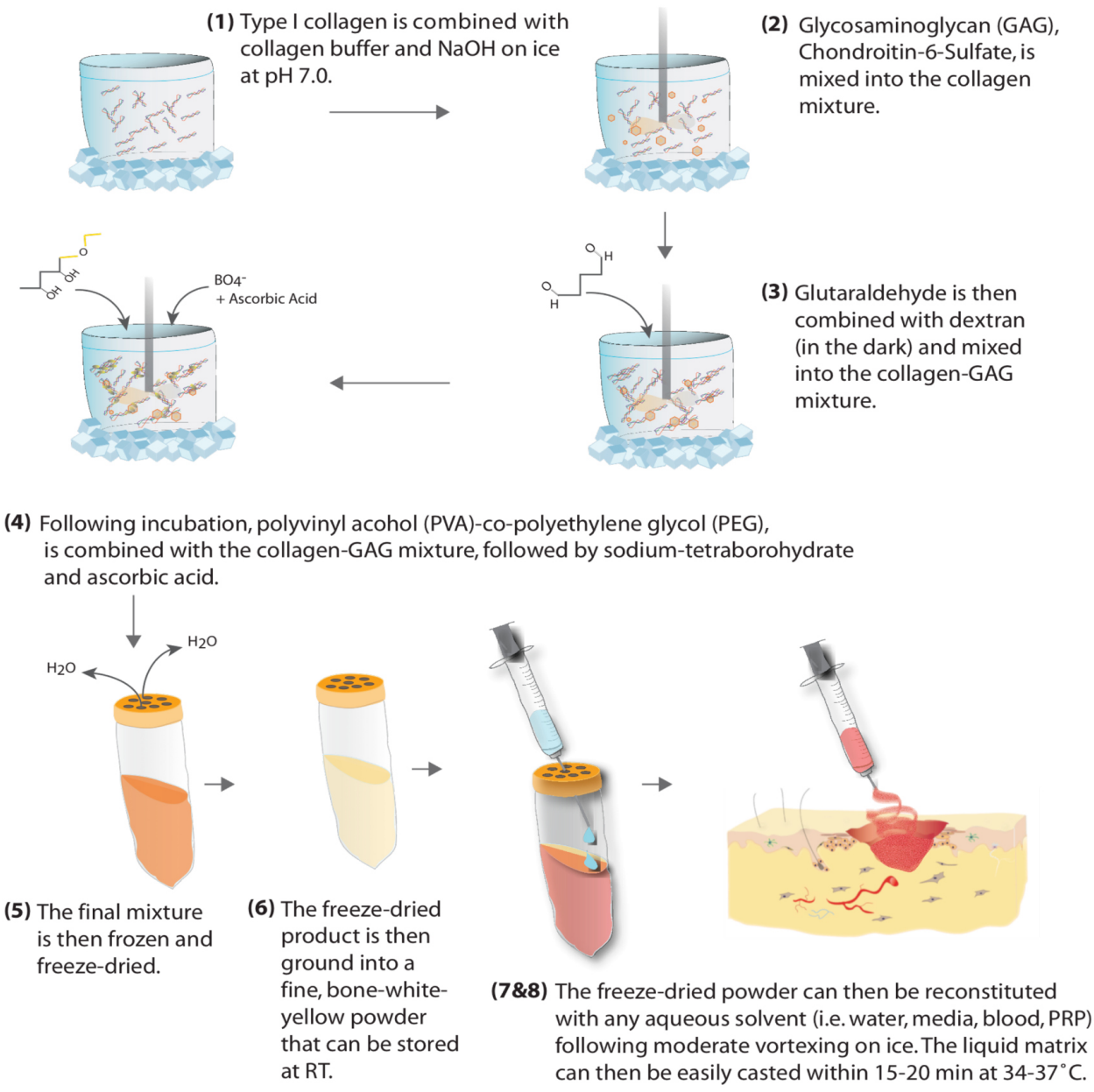


**Figure 2.1. Hydrogel fabrication.** The following procedure explains the process of synthesizing, freeze-drying, and reconstituting hydrogel in distilled water to apply on wound bed or in cell culture. Adopted from Hartwell et al., Biomedical Materials, 2016. Permission obtained (90).

### 2.2.2 Animal model- anesthesia and handling

All animals in this study were employed in accordance with protocols approved by the University of British Columbia (approval number: A12-0296). Following quarantine and clicker training, four female Yorkshire pigs (20-30 kg) were fasted for 18-24 hours with free access to water prior to surgery. Pigs were then anesthetized using a combination of ketamine and midazolam induction, and isoflurane maintenance. Propofol was added as needed to decrease isoflurane requirements. Prior to wound generation, buprenorphine (0.02-0.05 mg/kg) was administered subcutaneously (SQ). During surgery, pigs were monitored with echocardiogram, pulse oximeter, capnography, temperature probe, and blood pressure monitor. With veterinary consult, buprenorphine (0.02-0.05 mg/kg SQ) and/or meloxicam (0.3 mg/kg) was administered as needed for pain management post-operatively for 3-5 days.

### 2.2.3 Animal model- wound excision model

Four Pigs were placed prone, and the dorsum of pigs were shaved and washed with chlorhexidine solution (5 mg/ml). Pig wounds were pre-marked with a surgical pen using a custom 4 x 4 cm flexible steel template and tattooed on the margins. Marked sites were injected with epinephrine-saline solution (1:1000) prior to wound generation. Five full-thickness wounds, spaced 2 cm apart, were excised with a scalpel on the apex of the curved dorsal surface proximal to the midline, on each side of the pigs (10 wounds/pig). Generated wounds were divided into: no treatment (NT) (n=8), MeshFill (MF) (n=8), meshed Skin graft (MS) (n=6), meshed skin graft combined with MeshFill (MS+MF) (n=8). Gels were pre-warmed in a 37 °C incubator for 10 minutes, and 1.6 mL

of gel was added to the wound bed of MS and MS+MF group to allow for gelation to occur *in-situ*. The results from MS and MS+MF groups will be discussed in Chapter 3.

### 2.2.4 Dressing changes and tissue processing

Wound site dressings were changed every 5 days until all wounds were closed (≈40-50 days). Wounds and donor sites were washed with saline and covered with Mepitel® film dressing. Moist gauze, followed by dry gauze was placed on top of this dressing. Wound sites were jacketed with 3M Reston™ Self-Adhering Foam, with sutures placed around the foam to affix the dressing layers and protect the wounds. To keep the underlying layers intact, an additional net (Surgilast® Tubular Elastic Dressing Retainer) was utilized and stapled to the adherent foam. The third level of coverage consisted of 3M VetWrap™ to exert a mild pressure on the wound and keep grafts attached to the wound bed. Finally, the edges of the wrapping were secured with elastomer tape circumferentially around the torso.

For consistency, on days 10 and 20, 4 mm punch biopsies were taken from the same areas (0.5 cm from the bottom left or top right edge) of the NT and MF groups. Animals were euthanized on day 60 according to our protocol approved by the UBC animal ethics committee. Immediately after euthanizing the pigs, another set of 10 mm punch biopsies were taken from 0.5 cm margin of adjacent healthy skin.

### 2.2.5 Analysis of wound surface area and scar formation

Wound surface area was assessed on days 10 and 20, and scar surface area was determined on the final time point of the study (day 60). Digital photographs of

wounds and scars were taken with Canon PowerShot SX710 HS. Rulers were placed beside wounds in each photograph as a reference for analysis. Surface area (measured in $cm^2$) of wounds were normalized to the initial wound surface area, and expressed as a percentage. Digital photographs were analyzed using the ImageJ software.

### 2.2.6 Histology

Tissues were fixed in 10% formalin overnight and paraffin blocks were used for histological evaluation. Sections 5 μm thick were cut and stained with hematoxylin and eosin (H&E). Slides were scanned with Lecia Aperio CS2 slide scanner for analysis.

### 2.2.7 Epithelialization

Epithelialization was quantified via histology and a clinically blinded evaluation on 10 and 20 days post-surgery. Histologically, wounds with an epidermal layer covering the width of 4 mm punch biopsies were considered closed, whereas wounds with either partial or no epidermal layer were considered open. Gross estimation of epithelialization was conducted by a blinded plastic surgeon using digital photographs of wounds.

### 2.2.8 Tissue cellularity

Slides stained with hematoxylin were scanned using Leica Aperio CS2, and 3-5 high power field (HPF) snapshots were taken at 200x using the Aperio Imagescope software. Tissue cellularity was quantified using ImageJ by setting a scale for the smallest nuclei as a reference, and counting cells through an automated output. Data generated from day 10 and 20 samples were normalized to healthy skin punch biopsies

taken from the rostral or caudal dorsum of pigs, and expressed as a percentage. Day 60 data was normalized to adjacent healthy skin cellularity, and expressed as a percentage.

### 2.2.9 Epidermal thickness

Using Aperio Imagescope software, 5 measurements were taken from the epidermis in the scar area and adjacent healthy skin for each replicate on day 60. Averages were taken from each sample, and utilized to estimate the epidermal thickness of each group. Epidermal thickness was normalized to the adjacent healthy skin and expressed as a percentage.

### 2.2.10 Immunohistochemistry

Tissue sections 5 μm thick were cut, deparaffinized, and rehydrated. Next, antigen retrieval was performed by cooking slides in Tris-EDTA buffer (100 mM tris base, 1 Mm EDTA, 0.05% tween 20, ph 9.0) for 20 minutes, followed by 30 minutes of cooling at room temperature. Slides were rinsed in distilled water, and cell membranes were penetrated using Tris-buffered saline containing 0.1% Triton-X 100 (0.1% TBS-T) for intracellular proteins. Slides were subsequently washed two times with 0.025% TBS-T and blocked with 10% normal goat serum and 5% bovine serum albumin (1:1) for one hour. Tissue sections were incubated with either CD31 (1:100 dilution, Abcam, ab28364), CD3 (1:150 dilution, Abcam, Ab16669), or α-smooth muscle actin (1:100 dilution, Abcam, Ab5694) overnight at 4°C. On the second day, sections were washed three times with 0.025% TBS-T, followed by 0.3% Hydrogen peroxide to minimize non-

specific binding of intracellular peroxidase. Sections were incubated with goat anti-mouse (1:1500 dilution, Vector Laboratories, BA-9200) or goat anti-rabbit biotinylated secondary antibody (1:1000 dilution, Vector Laboratories, BA-1000), rinsed three times with 0.025% TBS-T, incubated with avidin-biotin complex (ABC) kit (Vector Laboratories, PK-6100) for 10 minutes, and developed with DAB peroxidase substrate kit (Vector Laboratories, SK-4100). Slides were counterstained with hematoxylin, dehydrated, and mounted using Permount™ mounting medium (Fisher Scientific). Three to five High-power field (HPF) images were taken at 200x from upper to lower dermis using Aperio Imagescope, and analyzed using the ImageJ software.

### 2.2.11 Statistical analysis

Data were expressed as mean ± standard error of the mean (SEM) of five or more independent observations. Statistical significance was calculated using a two-tailed unpaired t-test or a Fisher's exact test. *P-values* < 0.05 were considered statistically significant.

## 2.3 Results

### 2.3.1 Cell viability

Prior to conducting the animal model for this study, we examined the viability of fibroblasts in MF. Fibroblasts were stained with a mixture of Calcein AM (green to indicate viability) and EthD-1 (red to indicate dead cells) to assess cytotoxicity. As shown in figure 2.2 A, the majority of fibroblasts remain viable up to the end-point of the study (14 days). Due to uncertainty associated with visualizing cell viability in 3D

matrices using inverted fluorescence microscopes, this experiment was repeated on day 4 using a confocal microscope with z-stack optical sections. As a positive control, 0.05% saponin was used to visualize dead cells in a 3D matrix (figure 2.2 B). As seen in panel B, the majority of fibroblasts stained positive for Calcein AM (green), indicating they are live and viable. Further, within this matrix, embedded fibroblasts had a characteristic spindle shape showing their attachment to the network of fibers present in this scaffold.

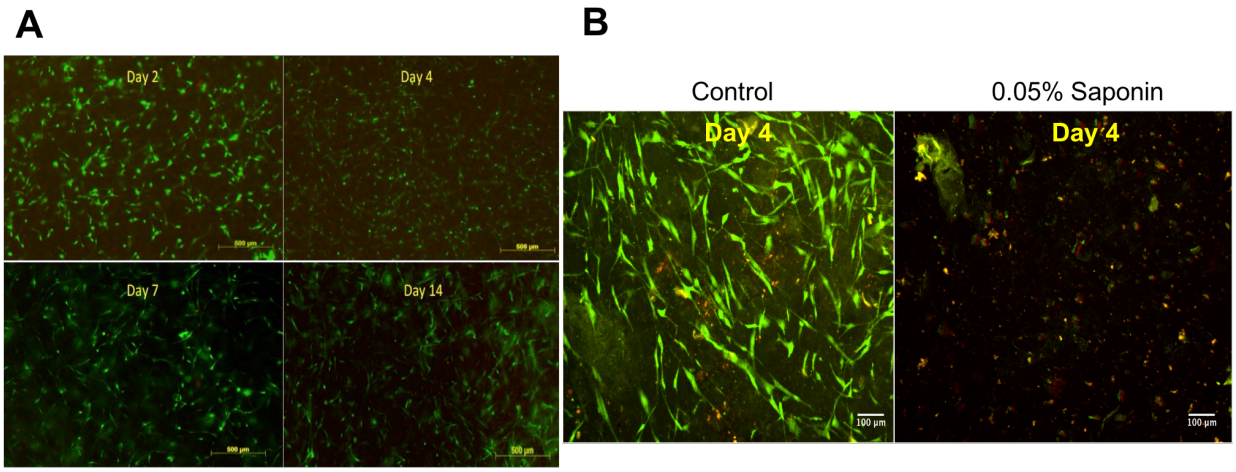


**Figure 2.2. Fibroblast viability in MeshFill.** (**A**) Viability of fibroblasts in MeshFill (MF) on days 2, 4, 7, and 14 using inverted fluorescence microscopy (green= live, red= dead) (n=3). (**B**) This assay was repeated on day 4 with 0.05% saponin as a positive control and imaged using confocal microscopy (n=3). Scale bars represent 500 µm (**A**) 100 µm (**B**).

### 2.3.2 Wound surface area

To assess whether healing occurred through contraction or epithelialization, we first examined wound surface area on days 10 and 20 post-surgery (figure 2.3 A,B).

Results from day 10 samples revealed no significant differences between MF-treated wounds and NT wounds (51.00 ± 5.93 vs 43.00 ± 4.76 %). However, the results from day 20 samples showed a significantly larger surface area of MF-treated wounds compared to NT wounds (23.01 ± 3.10 vs 13.83 ± 2.12 %, $p = 0.01$).

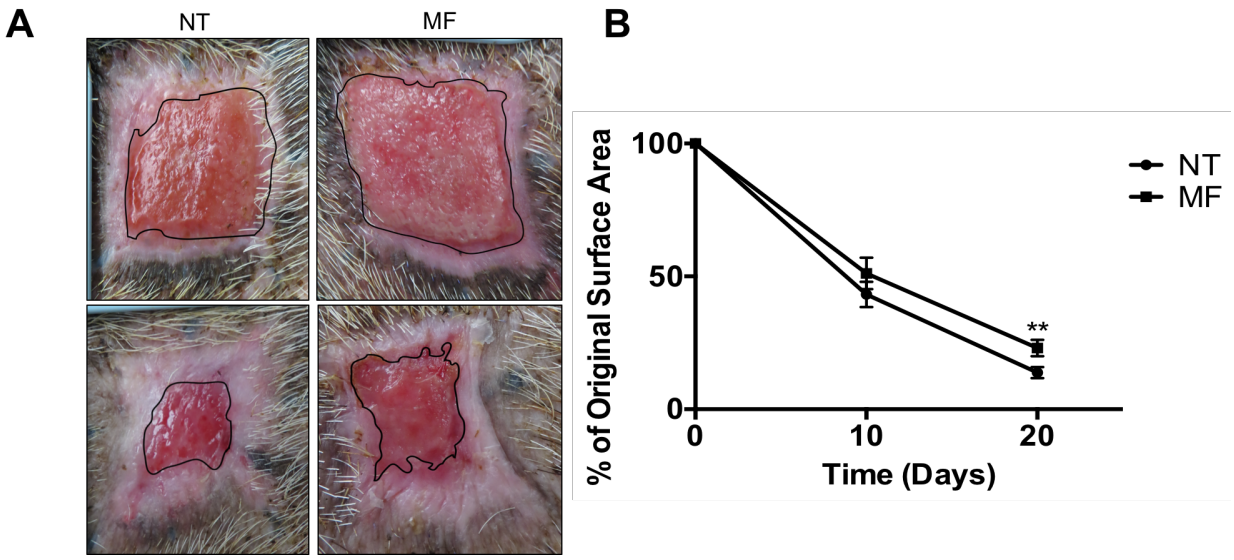


**Figure 2.3. Quantification of wound surface area.** (**A**) Clinical appearance of no treatment (NT) and MeshFill (MF) wounds on days 10 and 20 post-surgery. (**B**) Corresponding quantification of wound surface area (n=7-8, $p = 0.01$).

### 2.3.3 Epithelialization

Histological evaluation of epithelialization showed that 25 % of the NT and MF punch biopsies were epithelialized by day 10 (figure 2.4 B). Interestingly, samples from day 20 punch biopsies revealed that 50% of MF-treated and 12.5 % of NT wounds were epithelialized (figure 2.4 A,C). However, no significant differences were observed in either day 10 or 20 samples with regards to histological evaluation of epithelialization. Further, a plastic surgeon blinded to wound photographs estimated the percentage of

epithelialization. Results revealed no significant differences in gross estimates of epithelialization (figure 2.4 D). However, the clinician noted that 12.5 % of MF-treated wounds and 62.5 % of NT wounds healed through contraction.

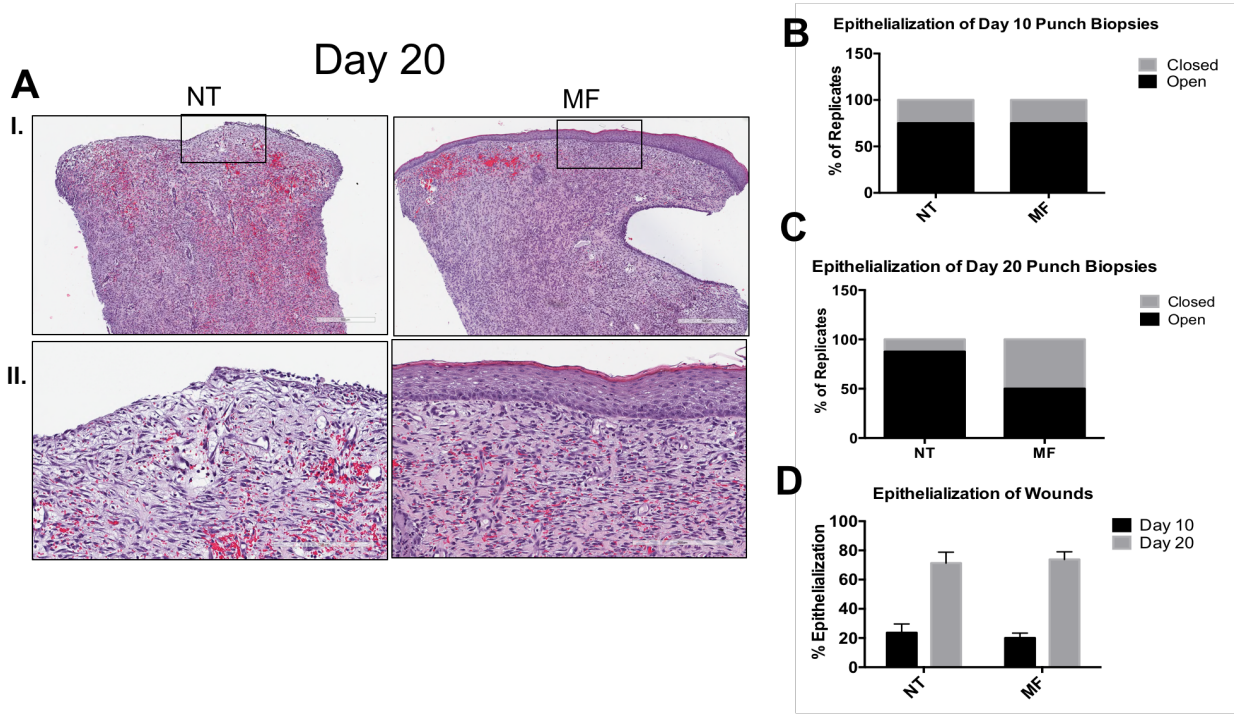


**Figure 2.4. Histological and clinical evaluation of epithelialization.** (**A**) Microscopic histology of no treatment (NT) and MeshFill (MF) groups 20 days post-surgery. (**B**,**C**) The percentage of closed (epithelialized) and open (not epithelialized) wounds on (**B**) day 10 and (**C**) day 20. (**D**) Blinded estimation of epithelialization using digital photographs (n=8, $p > 0.05$). Scale bars represent (**I.**) 500 µm and (**II.**) 200 µm

### 2.3.4 Tissue cellularity

Tissue cellularity was examined through HPF images of punch biopsies stained with hematoxylin (figure 2.5 A-D). The results showed no significant differences in tissue cellularity between MF-treated wounds and NT wounds on day 10 (391.85 ± 23.72 vs

415.15 ± 32.61 %) and day 20 (319.44 ± 13.02 vs 342.77 ± 43.07 %) samples when normalized to healthy skin (figure 2.5 A,B). Although not significant, the tissue cellularity of MF-treated samples taken on day 60 were 20 % lower than NT wounds (118.31 ± 14.01 vs 149.17 ± 24.87 %) when normalized to adjacent healthy skin.

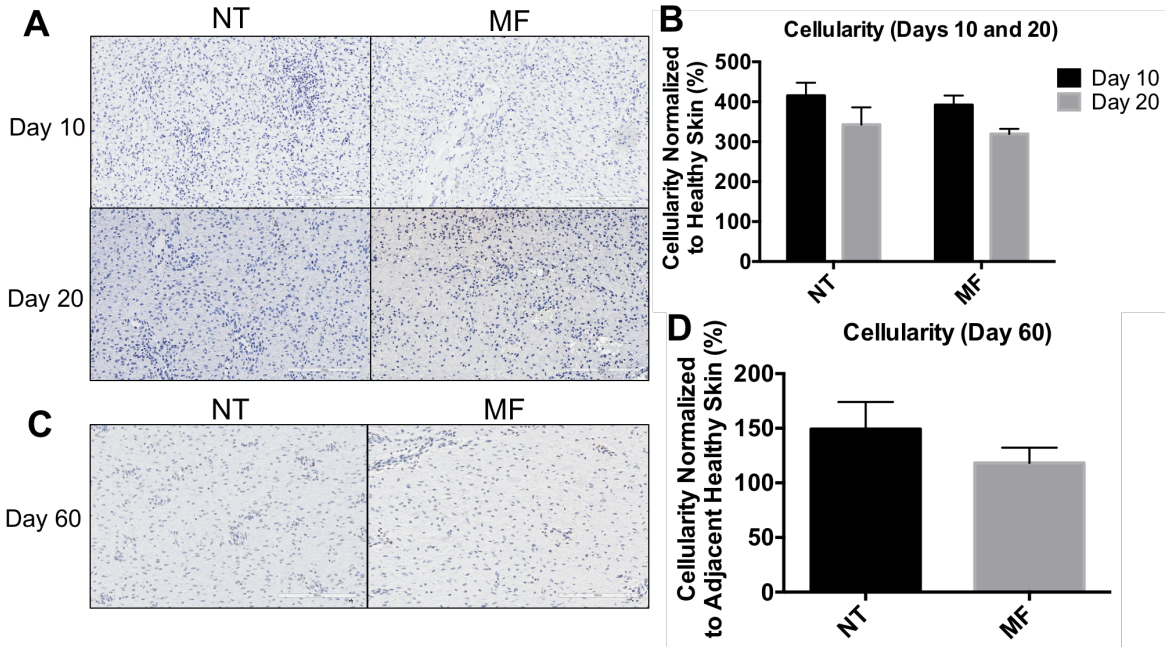


**Figure 2.5. Quantification of tissue cellularity on days 10, 20, and 60 post-surgery.** (**A,C**) Photomicrograph images of hematoxylin staining depicting cellularity in no treatment (NT) and MeshFill (MF) groups on days 10, 20, and 60. (**B**,**D**) Corresponding quantification of dermal cellularity on days 10, 20, and 60 (n=5-8, $p > 0.05$). Scale bars represent 200 μm.

### 2.3.5 CD31 immunohistochemistry

The presence of vessel-like structures was examined in wounds by staining tissue sections for the endothelial cell marker cluster differentiation 31 (CD31) (figure

2.6). The results of samples taken on day 10 post-surgery showed no significant differences between the number of vessel-like structures in MF-treated and NT wounds (23.55 ± 1.34 vs 27.77 ± 2.67 vessels/HPF). However, a marginal reduction in vessel-like structures of MF-treated wounds was observed in day 10 samples. Further, there were no significant differences in the number of vessel-like structures in MF-treated and NT wound samples taken on day 20 (20.20 ± 2.62 vs 20.63 ± 3.00 vessels/HPF).

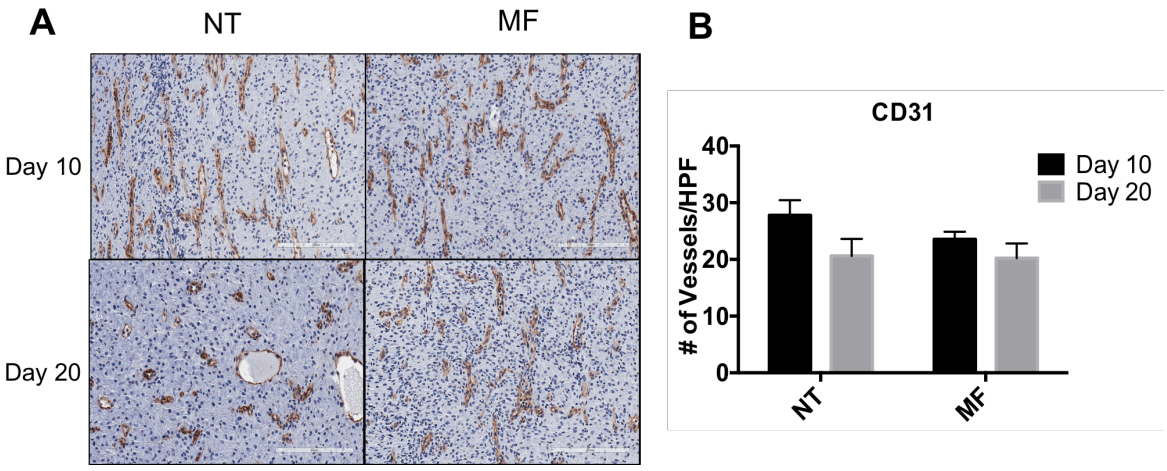


**Figure 2.6. Quantification of vessel-like structures in the dermis on days 10 and 20 post-surgery.** (**A**) Photomicrograph images and (**B**) corresponding quantification of CD31 immunohistochemistry showing vessel-like structures in the dermis of no treatment (NT) and MeshFill (MF) samples on days 10 and 20 (n=6-8, $p > 0.05$). Scale bars represent 200 µm.

### 2.3.6 CD3 immunohistochemistry

Infiltration of T-lymphocytes was evaluated in wounds using CD3 immunohistochemistry. The results shown in figure 2.7 (A-C) revealed that wounds

treated with MF had a 30 % reduction in $CD3^+$ T cells compared to NT wounds (6.39 ± 0.88 vs 9.12 ± 1.45 %) on day 10, and a 23 % reduction (7.01 ± 0.61 vs 9.13 ± 1.45 %) in $CD3^+$ T cells in day 20 samples. However, these differences were not significant on both day 10 and 20 samples.

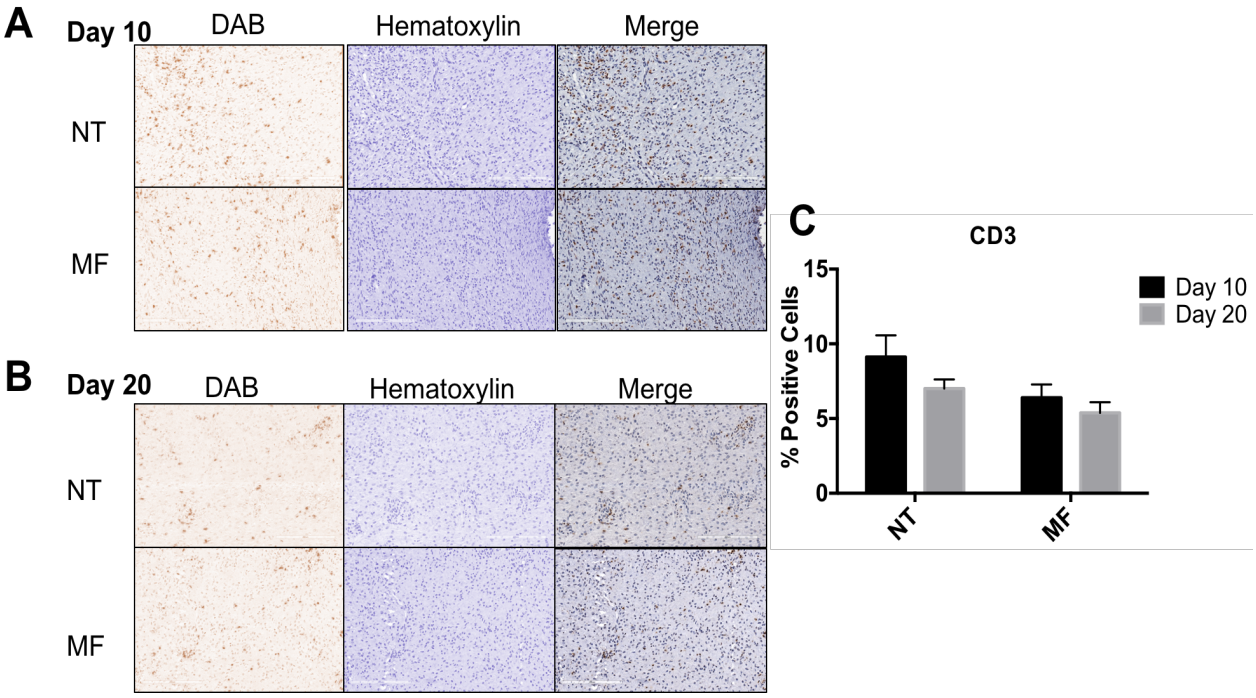


**Figure 2.7. Quantification of T-lymphocytes in the dermis on days 10 and 20 post-surgery.** (**A,B**) Photomicrograph images show merged and color deconvoluted images depicting diaminobenzidine (DAB) staining for CD3 T-lymphocytes and hematoxylin staining showing nuclei in no treatment (NT) and MeshFill (MF) group. (**C**) Corresponding quantification of $CD3^+$ cells in the dermis (n=5-8, $p > 0.05$). Scale bars represent 200 µm.

### 2.3.7 α-SMA immunohistochemistry

Due to the differences in wound areas seen in figure 2.3, we were interested to examine the presence of myofibroblasts in tissue samples using α-SMA staining. As seen in figure 2.8 (A,B), the upper dermis showed a high number of vessel-like structures strongly stained with α-SMA. The majority of cells present within the middle to lower dermis stained positive for α-SMA on both days 10 and 20. Qualitatively, no differences in the number of α-SMA expressing cells in MF-treated wounds and NT wounds were observed in day 10 or day 20 samples.

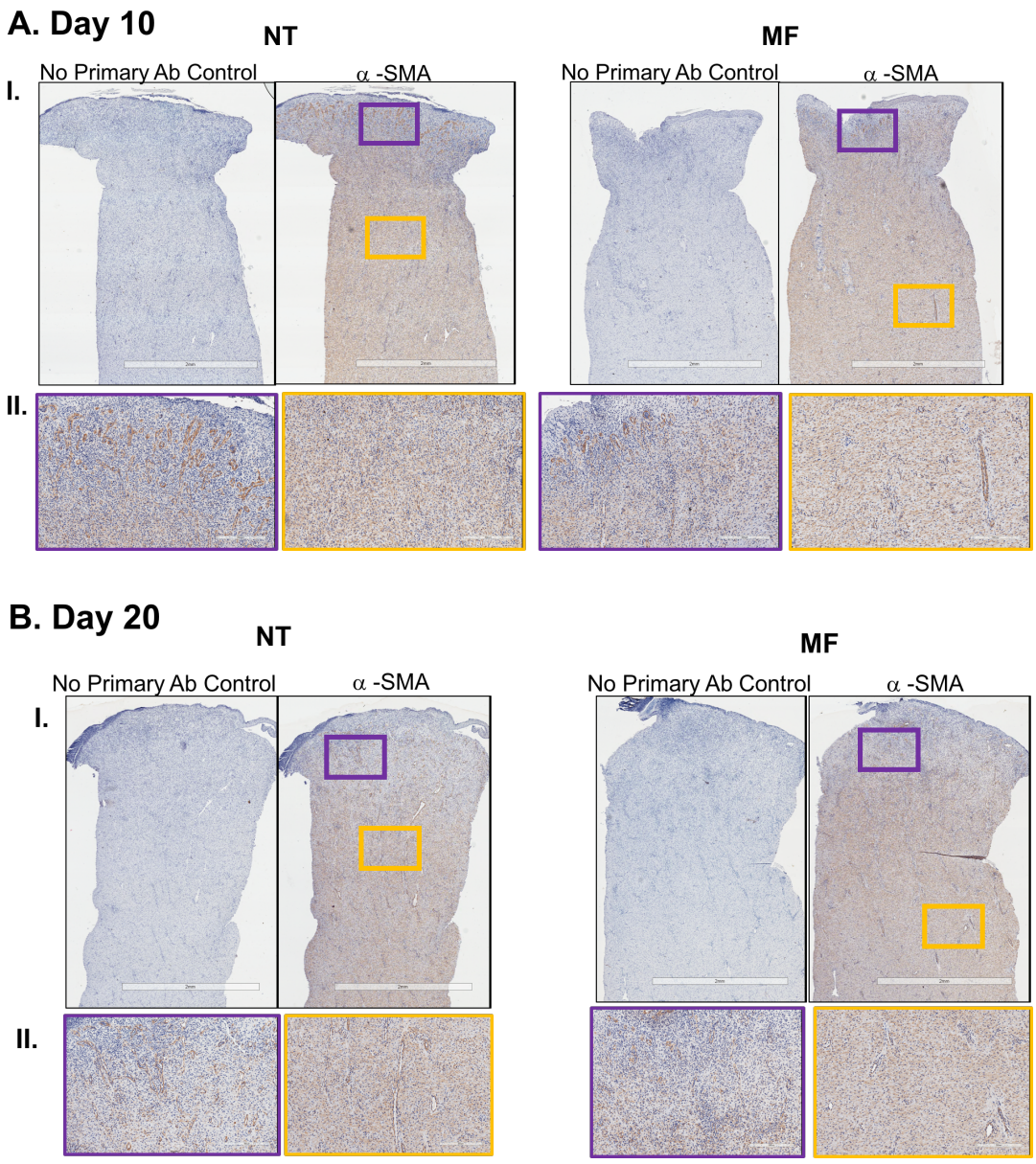


**Figure 2.8. Presence of dermal myofibroblasts on days 10 and 20 post-surgery.** (**A**) **I.** Photomicrograph images showing α-SMA immunohistochemistry and no primary antibody (Ab) control in no treatment (NT) and MeshFill (MF) groups at 20x magnification. **II.** Corresponding color-coded magnifications at 200x showing α-SMA staining in the upper and lower dermis. Scale bars represent (**I.**) 2 mm and (**II.**) 200 μm (n=8).

### 2.3.8 Scar surface area

Scar surface areas were examined 60 days after surgery (Figure 2.9 A,B). The results showed no significant differences in the scar surface area of MF-treated groups when compared to NT wounds (4.15 ± 0.384 vs 4.54 ± 0.38 $cm^2$).

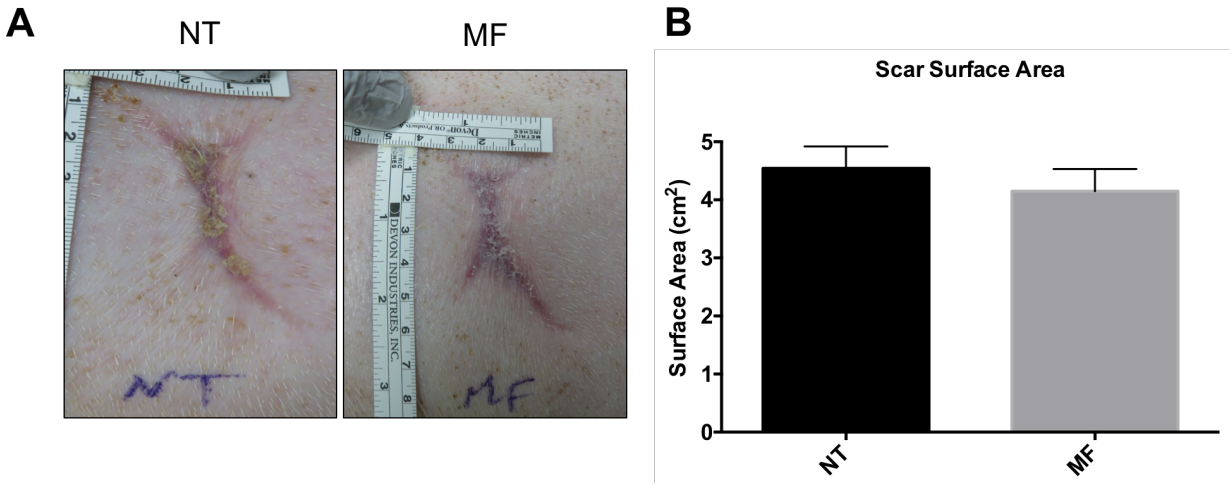


**Figure 2.9. Scar surfaces area analysis 60 days post-surgery.** (**A**) Digital photographs of scars shown on day 60 in no treatment (NT) and MeshFill (MF) groups. (**B**) Corresponding quantification of scar surface area (n=8, $p > 0.05$).

### 2.3.9 Epidermal thickness

Hematoxylin and eosin (H&E) stained tissue were examined to determine epidermal thickness 60 days after surgery (Figure 2.10 A,B). Though not significant, MF-treated wounds epidermal thickness was 15% lower than NT wounds and more comparable to adjacent healthy skin (140.00 ± 9.22 vs 165.00 ± 18.53 %).

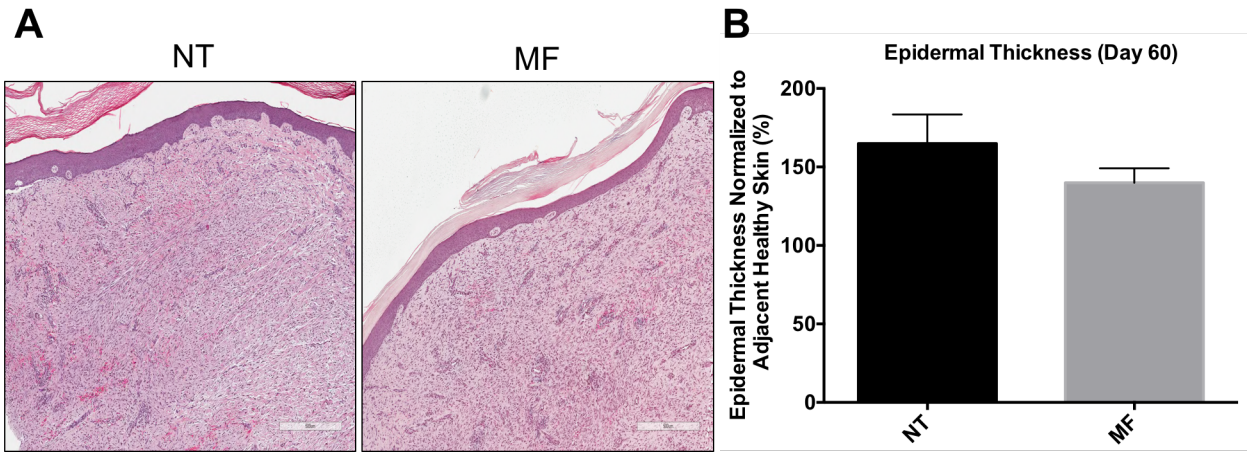


**Figure 2.10. Epidermal thickness 60 days post-surgery.** (**A**) Photomicrograph histology images showing epidermal thickness of no treatment (NT) and MeshFill (MF) groups. (**B**) Corresponding quantification of epidermal thickness on day 60 (n=5-7, $p > 0.05$). Scale bars represent 500 μm.

## 2.4 Discussion

It is well known that severe injuries, such as full-thickness burns, require early excision of burn wound eschar and timely wound coverage (104). Failing to meet these needs may make the wound vulnerable to infection, water and heat loss, and prone to hypertrophic or excessive scarring (104, 105). An ideal skin substitute should provide a moist environment and serve as a provisional matrix, allowing fibroblast and keratinocyte migration to facilitate rapid epithelialization and extracellular matrix production while minimizing scar formation (105).

The field of tissue engineering has erupted with various types of skin substitutes to address these factors. As previously mentioned, most of these skin substitutes are manufactured in a pre-formed sheet, making them undesirable and inefficient for clinical

use (90). In order to address the needs for a clinically suitable skin substitute, our group has designed a tissue compatible, *in-situ* forming hydrogel to serve as a provisional matrix in healing wounds. In this pilot study, we examined the application of this hydrogel in full-thickness wounds in a porcine model.

Our lab has previously shown that fibroblast cell cultures with MF resisted contraction when compared to a standard collagen-GAG scaffold over a 7-day period (92). Similarly, in this chapter, we showed that the application of MF significantly resisted contraction on day 20 post-surgery (figure 2.3 B). Interestingly, these results did not translate when the presence of myofibroblasts were examined qualitatively through α-SMA immunohistochemistry (figure 2.8 A,B). As the quantification of this data was prone to error due to the immense number of α-SMA$^{+}$ cells throughout the dermis, a suitable way to quantify this data in the future is through measuring fluorescence intensity (106). These results could provide insight into *in-vivo* cellular mechanisms of resistance to contraction when applying MF.

In this chapter, it was found that 50% of punch biopsies taken from the MF group on day 20 showed complete epithelialization compared to only 12.5% in NT wounds (figure 2.4 A,C). These differences prompted our group to quantify epithelialization of the entire wound using digital photographs. However, when the percentage of epithelialization was quantified by a blinded plastic surgeon, MF-treated wounds did not reveal significant differences compared to the NT group. A potential reason for this observation may be due to the small amount of hydrogel applied to the wound bed. Based on histological measurements, the mean dermal thickness from healthy dorsal skin was 4.96 ± 0.28 mm (n=12). The volume of hydrogel added (1.6 mL) represents

only 20.17% of the wound cavity. Thus, the therapeutic benefit of the hydrogel may be underscored due to the minute amount of gel added.

Other potential reasons for the lack of differences in epithelialization of MF-treated wounds is the dehydration rate of hydrogel scaffolds. As PVA is a well-known polymer utilized in hydrogels, previous studies using varying concentrations of a PVA-based hydrogel have indicated that the thickness of gel added is inversely related to the dehydration rate (107). Thus, hydrogels containing PVA-based polymers should be reapplied at frequent intervals to prevent rapid drying of the wound bed. Indeed, in our previous study using the rabbit ear model of hypertrophic scars, wound cavities were completely filled with MF, and additional amounts of hydrogel was reapplied daily for the first 4 out of 35 days of the study. The results showed an improved healing outcome in scar elevation index, cellularity, and vascular perfusion and innervation. Ideally, future studies should examine the dehydration and degradation rate of MF to minimize the number of dressing changes and hydrogel reapplication.

In this chapter, we also examined tissue cellularity and identified the types of cells present in wounds over the course of the study (figures 2.5-2.8). As previously mentioned, the majority of cells in the dermis comprised of myofibroblasts in both NT and MF-treated groups (figure 2.8 A,B). Further, we reported that MF-treated wounds showed a pattern towards decreased tissue cellularity in day 60 samples (figure 2.5 D). Similar patterns were observed in MF-treated wounds with regards to the number of vessel-like structures (figure 2.6 A,B) and T-lymphocytes on day 10 (figure 2.7 A,B). Thus, a possible explanation for these observations is that the presence of MF in the first 10 days post-surgery accelerated the inflammatory phase and regression of blood

vessels, but the degradation of MF over time ceased these outcomes. However, to validate these propositions, fluorescent labelling of MF, in addition to evaluating inflammation and vascularization at earlier time points (day 3 to 5) is required.

Without the use of skin grafts, scar formation is inevitable in large full-thickness wounds. In figure 2.3 (A,B), we showed that MF significantly resisted contraction on day 20. As a result, we examined whether resistance to contraction would persist, leading to a reduced scar surface area during the remodeling phase of wound healing. As seen in figure 2.9 (A,B), MF-treated wounds revealed a marginally lower scar surface area compared to NT group, but this difference was not significant. Additionally, the epidermal thickness of MF-treated wounds was relatively lower than NT wounds and more comparable to healthy skin (Figure 2.10 B). Based on these patterns, it would be interesting for future studies to explore mechanisms leading to these results.

In conclusion, this pilot study has revealed the potential of an *in-situ* forming hydrogel for treatment of full-thickness wounds. The application of minute amounts of MF showed patterns in improved wound healing outcomes. A major limitation of this study was the amount of hydrogel added to the wound bed, which could become dehydrated or degraded, masking potential therapeutic benefits of MF. Based on the patterns seen from this study, we hypothesize that reapplication of MF during dressing changes could lead to better healing outcomes. Nonetheless, in the case of full-thickness wounds, the use of liquid scaffolds alone is not sufficient, and skin grafts are required. In the next chapter, we will examine the aesthetic and wound healing outcomes when combining split-thickness MSGs with MF.

# Chapter 3: Evaluating the aesthetic and wound healing outcomes of a combination of split-thickness meshed skin grafts and an in-situ forming hydrogel in full-thickness excisional wounds

## 3.1 Introduction

Patients suffering from burn injuries are not only affected physically, but their mental well-being is also compromised. Previous studies have shown an association between the extent of burn injury (superficial or deep burns), anxiety, and depression (108). Further, patients from the ages of 5-18 years have reported decreased happiness and life satisfaction with increasing number of visible scars (109).

The current gold-standard of care for large burn injuries is the split-thickness meshed skin graft (MSG) (75). Developed by Tanner and Vandeput in the 1960s, MSGs offered a convenient method for skin expansion in cases where the donor site availability was limited (50). Meshed skin grafts can conform to irregular surfaces of the wound bed (75). Additionally, the perforations present in MSGs permit fluid drainage, thereby ensuring better graft take and increasing resistance to infections (80). However, the perforated sites contract as granulation tissue develops, ultimately leading to aesthetically undesirable outcomes.

Previous studies examining healing of MSGs in pre-clinical animal models have primarily utilized cultured keratinocytes to accelerate epithelialization (110, 111). A study done by Sharpe's group found that the combination of cultured keratinocytes and MSGs accelerated epithelialization and reduced contractures in large white pigs (110). Comparably, another study conducted on a rat animal model found that faster

epithelialization occurred when using cultured keratinocytes with MSGs (111). However, in these articles, the authors did not report differences in the aesthetic outcomes of healing when cultured keratinocytes were combined with MSGs. In addition, the practical application of cultured keratinocytes in clinics are questionable as it is expensive, time-consuming, and requires a laboratory specialist (110).

As a result, other methods in improving healing and aesthetic outcomes of MSGs should to be explored. To date, the aesthetic outcomes of fishnet-like scarring in MSGs is understudied in pre-clinical animal models. Therefore, in this chapter, we examined whether the combination of autologous MSGs plus our liquid scaffold, MeshFill (MF), improved wound healing and aesthetic outcomes of full-thickness wounds in a pre-clinical porcine model.

### 3.2 Methods

For details on the animal model, dressing changes, wound surface area analysis, and immunohistochemistry, please refer to Chapter 2 (section 2.2).

#### 3.2.1 Harvesting and meshing skin grafts

Donor sites (maximum 4 x 9 cm on each side) were generated along the pig's rib cage using a Zimmer® electric dermatome with a 2" guard set at a thickness of 20/1000 inches (0.508 mm). The harvested skin was placed on a sterile, disposable carrier, and meshed in a 3:1 ratio using the Zimmer® skin mesher. Meshed skin (MS) was subsequently cut into sized-matched pieces corresponding to the wound with 10% overlap on the edges, and stapled onto the wound margins. Eight replicates from the

MS+MF group received 1.6 mL of MF, a sufficient amount to fill the void areas of meshed skin grafts. Gels were pre-warmed in a 37 °C incubator for 10 minutes and added to the wound bed to allow gelation to occur *in-situ*.

### 3.2.2 Evaluation of aesthetic outcomes

Five evaluators, comprised of a dermatologist and four medical students, were given a learning module providing background information on the objectives of the study and detailing the outcome variables being assessed in this evaluation. Participants were blinded to digital photographs of MS and MS+MF groups on day 60, and asked to evaluate the following three variables after reviewing the learning module: clinical appearance, contracture, and redness of wounds. Scores ranged from 1 to 5, and the higher the score, the better the outcome, with the exception of contractures, where a higher score indicated an increased subjective evaluation of contractures. With each of the three variables, the learning module described the problem (e.g. the appearance of fishnet like scars when examining clinical appearance) and provided example images. Further, the evaluators were also asked to examine all wounds before scoring each digital photograph of wounds individually, thereby providing a relative score for each image. The scores of each evaluator was summed and divided by the highest possible score to provide results expressed as percentages (e.g. given 6 images scored from 1 to 5, the highest possible score would be 30). This was done for both MS and MS+MF groups. The mean score for a variable was taken among evaluators and reported as mean ± standard error of the mean (SEM).

### 3.2.3 Tissue cellularity

Due to the lack of a flattened epidermis and uncertainty with discerning scar tissue, hematoxylin and eosin (H&E) staining was used to localize scar tissue present in the MS and MS+MF groups on day 60. Tissue cellularity was assessed as described in Chapter 2 (section 2.2.8)

### 3.2.4 Epidermal and dermal thickness

Using Aperio Imagescope software, 5 measurements were taken from the epidermis and 3 measurements from the dermis in the scar area and adjacent healthy skin of day 60 samples. Averages were taken from each sample, and utilized to estimate the epidermal and dermal thickness of each group. Both epidermal and dermal thicknesses were normalized to the adjacent healthy skin and expressed as a percentage.

### 3.2.5 Statistical analysis

Data were expressed as mean ± (SEM) with five or more independent observations. Statistical significance was calculated using a two-tailed paired t-test for evaluation of aesthetic outcomes, and an unpaired t-test for wound surface area, immunohistochemistry, cellularity, and epidermal and dermal thickness. *P-values* $< 0.05$ were considered statistically significant.

## 3.3 Results

### 3.3.1 Evaluation of aesthetic outcomes

Three variables were assessed in these evaluations: clinical appearance, contracture, and redness (figure 3.1 A,B). As shown in panel A, the clinical appearance of MS+MF groups markedly improved when compared to MS wounds. Blinded evaluations of wounds confirmed this observation, demonstrating significantly higher scores on clinical appearance of the MS+MF photographs when compared to the MS group (74.00 ± 4.51 vs 63.33 ± 4.60 %, $p = 0.04$) (figure 3.1 B I.). Similarly, contractures were significantly reduced in the MS+MF photographs when compared to that of the MS group (28.50 ± 3.50 vs 40.67 ± 4.64 %, $p = 0.007$) (figure 3.1 B II.). However, the wound redness (figure 3.1 B III.) did not differ significantly for the MS+MF photograph evaluations when compared to the MS group (61.50 ± 4.85 vs 64.00 ± 2.87%).

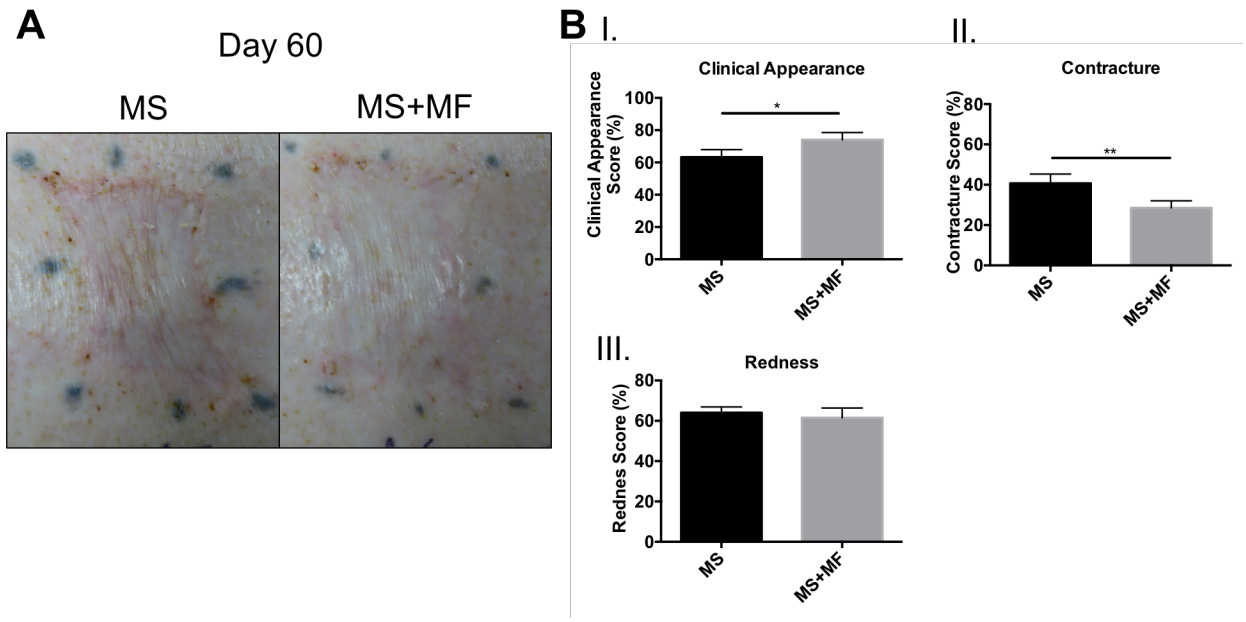


**Figure 3.1. Blinded evaluations of aesthetic outcomes 60 days post-surgery** (**A**) Clinical appearance of meshed skin (MS) and meshed skin + MeshFill (MS+MF) group on day 60. (**B**) Quantified scores of blinded evaluators expressed as percentages (n=5). Categories include (**I.**) clinical appearance ($p$ = 0.04), (**II.**) contracture ($p$ = 0.007), and (**III.**) redness ($p$ > 0.05).

### 3.3.2 Wound surface area

Surface area of wounds were quantified ($cm^2$), normalized to the initial surface area, and expressed as percentages (figure 3.2 A,B). Although the results showed no significant differences between MS+MF and MS-treated wounds on day 10 (81.76 ± 4.10 vs 73.95 ± 7.65 %), day 20 (76.16 ± 4.76 vs 66.04 ± 3.17 %) and day 60 samples (92.57 ± 6.88 vs 80.70 ± 7.44), the MS+MF wounds remained relatively less contracted at all time points when compared to MS alone. Interestingly, on day 60, the overall

surface area of MS+MF and MS-treated wounds increased, reaching close to the surface area excised at the beginning of the study (figure. 3.2 B).

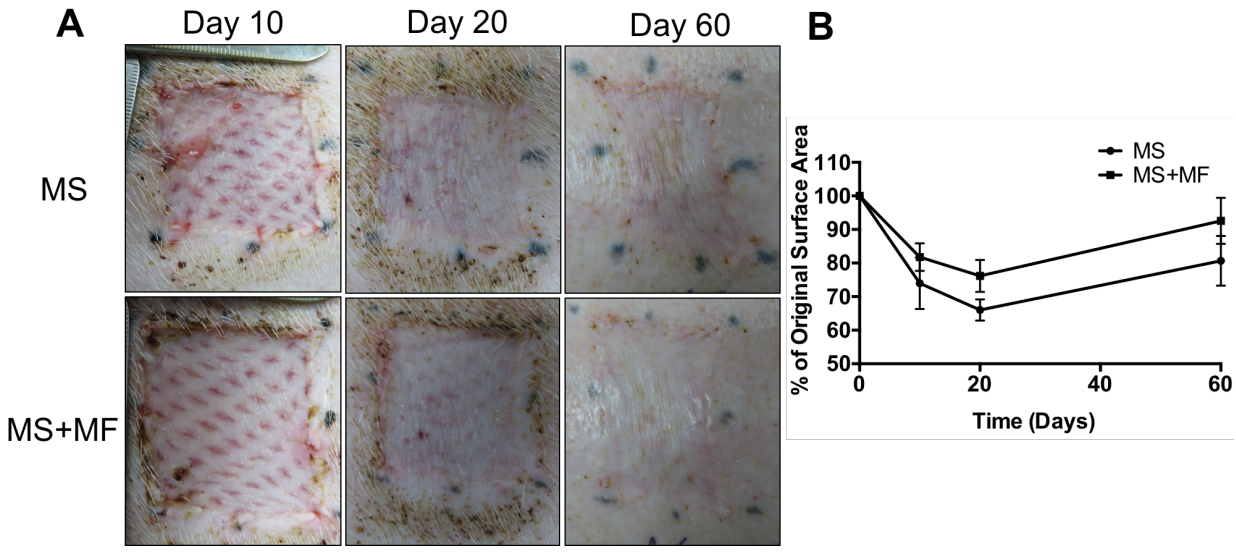


**Figure 3.2. Contracture analysis of wounds on days 10, 20, and 60 post-surgery.** (**A**) Clinical appearance showing contracture of meshed skin (MS) and meshed skin + MeshFill (MS+MF) over time. (**B**) Corresponding quantification of wound surface area (n=6-8, $p > 0.05$).

### 3.3.3 Tissue cellularity

Cellularity was examined through high power field (HPF) images of punch biopsies stained with hematoxylin for day 10 and 20 samples (figure 3.3 A,B), and H&E for day 60 samples (figure 3.3 C,D). The results showed no significant differences in tissue cellularity of wounds treated with MS+MF or MS groups on day 10 (273.75 ± 16.72 vs 266.72 ± 19.94 %), day 20 (223.58 ± 24.03 vs 225.34 ± 23.66 %) (figure 3.3 A,B), and day 60. However, there was nearly a 10% reduction in tissue cellularity of

MS+MF compared MS-treated wounds in day 60 samples (262.20 ± 15.54 vs 289.20 ± 49.77 %) (figure 3.3 C,D).

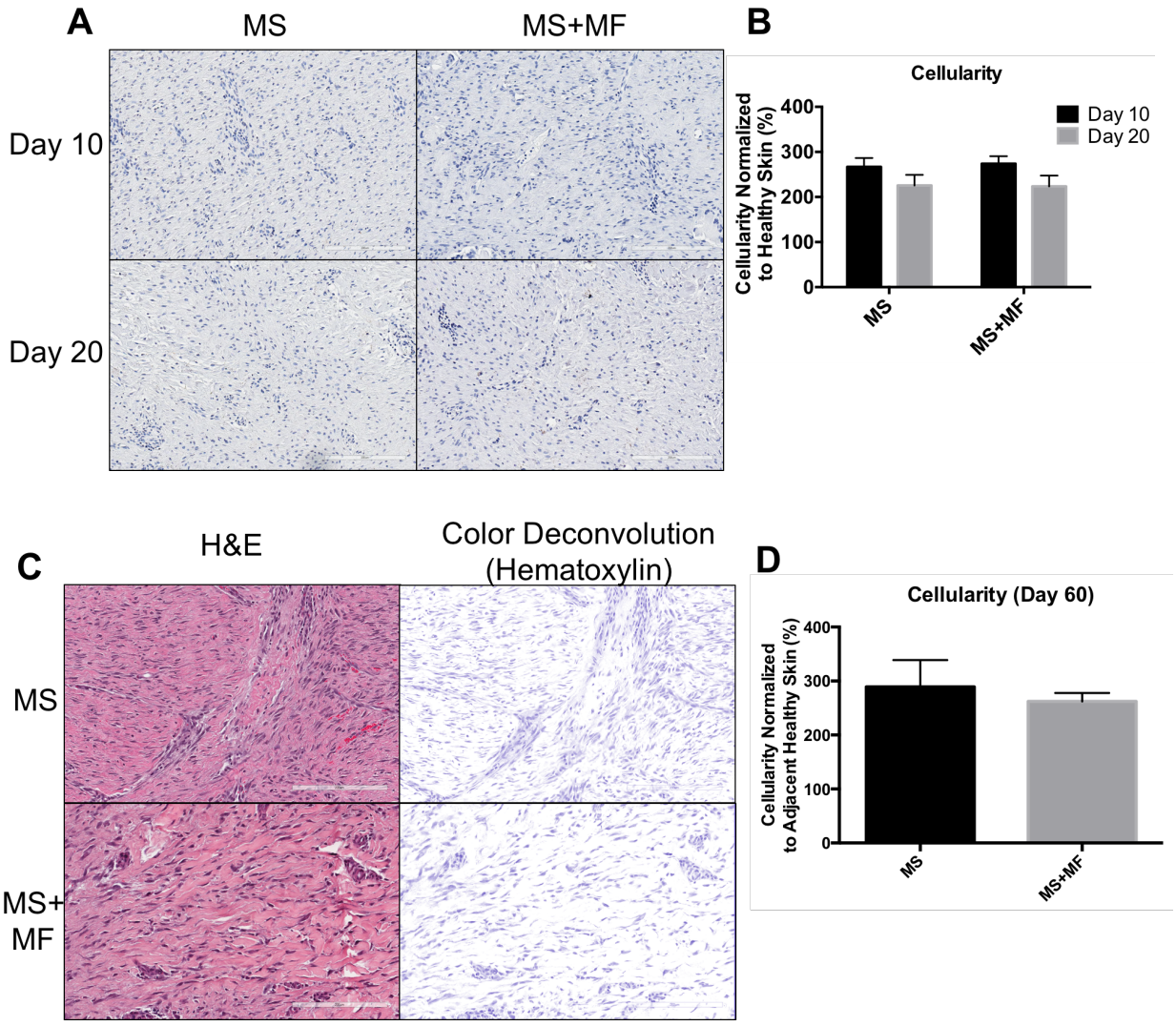


**Figure 3.3. Quantification of tissue cellularity on days 10, 20, and 60 post-surgery.** (**A**) Representative photomicrographs hematoxylin staining images and (**C**) H&E images depicting cellularity of meshed skin (MS) and meshed skin + MeshFill (MS+MF) group on days 10, 20, and 60. (**B**,**D**) Corresponding quantification of dermal cellularity on days 10 and 20 (n=6-8, $p > 0.05$). Scale bars represent 200 μm.

### 3.3.4 CD31 immunohistochemistry

The presence of vessel-like structures was examined in wounds by staining for endothelial cell marker cluster differentiation 31 (CD31). As shown in figure 3.4 (A,B), the MS+MF-treated wounds showed a significant reduction in the number of vessel-like structures when compared to the MS samples (18.44 ± 1.92 vs 13.07 ± 1.41 vessels/HPF, $p$ = 0.04) 10 days post-surgery. However, there was no significant differences in the number of vessel-like structures in the MS+MF and MS-treated wounds (12.43 ± 1.79 vs 12.08 ± 2.84 vessels/HPF) on day 20.

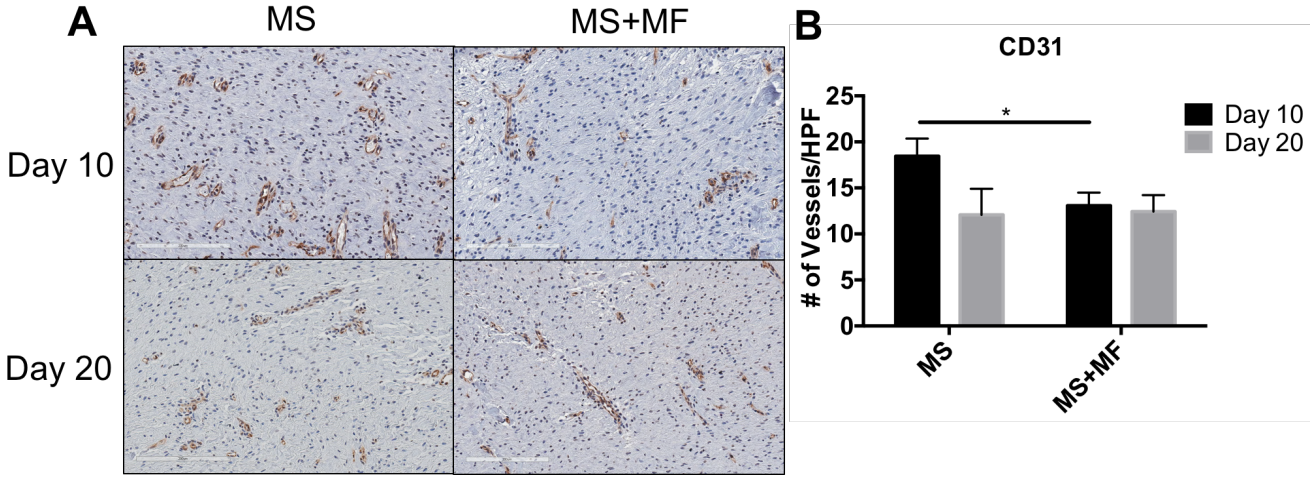


**Figure 3.4. Quantification of vessel-like structures in the dermis on days 10 and 20 post-surgery.** (**A**) Photomicrograph images and (**B**) corresponding quantification of CD31 immunohistochemistry showing vessel-like structures in the dermis of meshed skin (MS) and meshed skin + MeshFill (MS+MF) samples on days 10 and 20 (n=5-8, $p$ = 0.04).

### 3.3.5 CD3 immunohistochemistry

Infiltration of T-lymphocytes in wounds was evaluated using CD3 immunohistochemistry. Though no significant differences were identified on day 10 (3.23 ± 0.52 vs 4.59 ± 0.61 %) and day 20 samples (1.77 ± 0.25 vs 1.62 ± 0.21 %), MS+MF-treated wounds had nearly 30% less $CD3^+$ T cells when compared to MS samples on day 10.

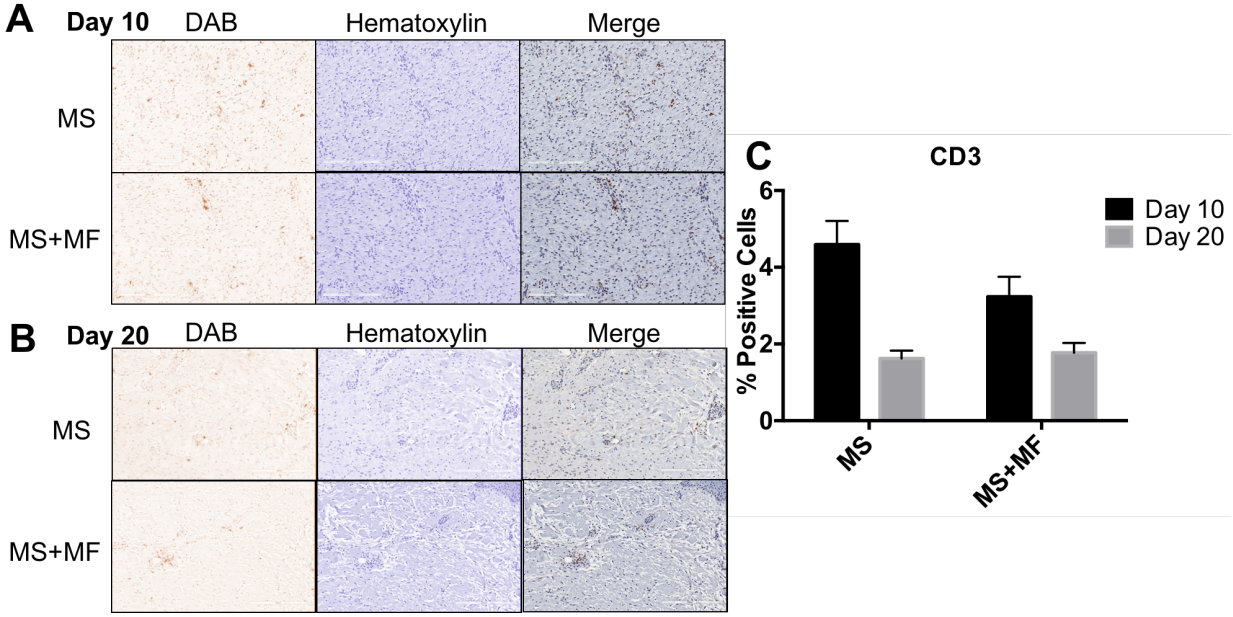


**Figure 3.5. Quantification of T-lymphocytes in the dermis on days 10 and 20 post-surgery.** (**A,B**) Photomicrograph images show merged and color deconvoluted images depicting diaminobenzidine (DAB) staining for CD3 T-lymphocytes and hematoxylin staining showing nuclei in meshed skin (MS) and meshed skin + MeshFill (MS+MF) groups. (**C**) Corresponding quantification of $CD3^+$ cells in the dermis (n=5-8, $p > 0.05$). Scale bars represent 200 μm.

### 3.3.6 α-SMA immunohistochemistry

Due to the differences observed in contracture evaluations between the MS+MF and MS-treated wounds (figure 3.1 A,B), we were interested in examining whether these results translated to differences in the number of dermal myofibroblasts using immunohistochemical staining for α-SMA . As shown in figure 3.6 A, the majority of cells in the upper dermis stained positive for α-SMA in the void areas for both MS+MF and MS-treated wounds. Similarly, the majority of cells in the middle to lower dermis stained positive for α-SMA. On day 20 (figure 3.6 B), both groups contained relatively reduced number of $\alpha\text{-SMA}^{+}$ cells, particularly in the upper dermis. From a qualitative standpoint, no differences or patterns were observed between the MS+MF and MS punch biopsies on both day 10 and 20 samples.

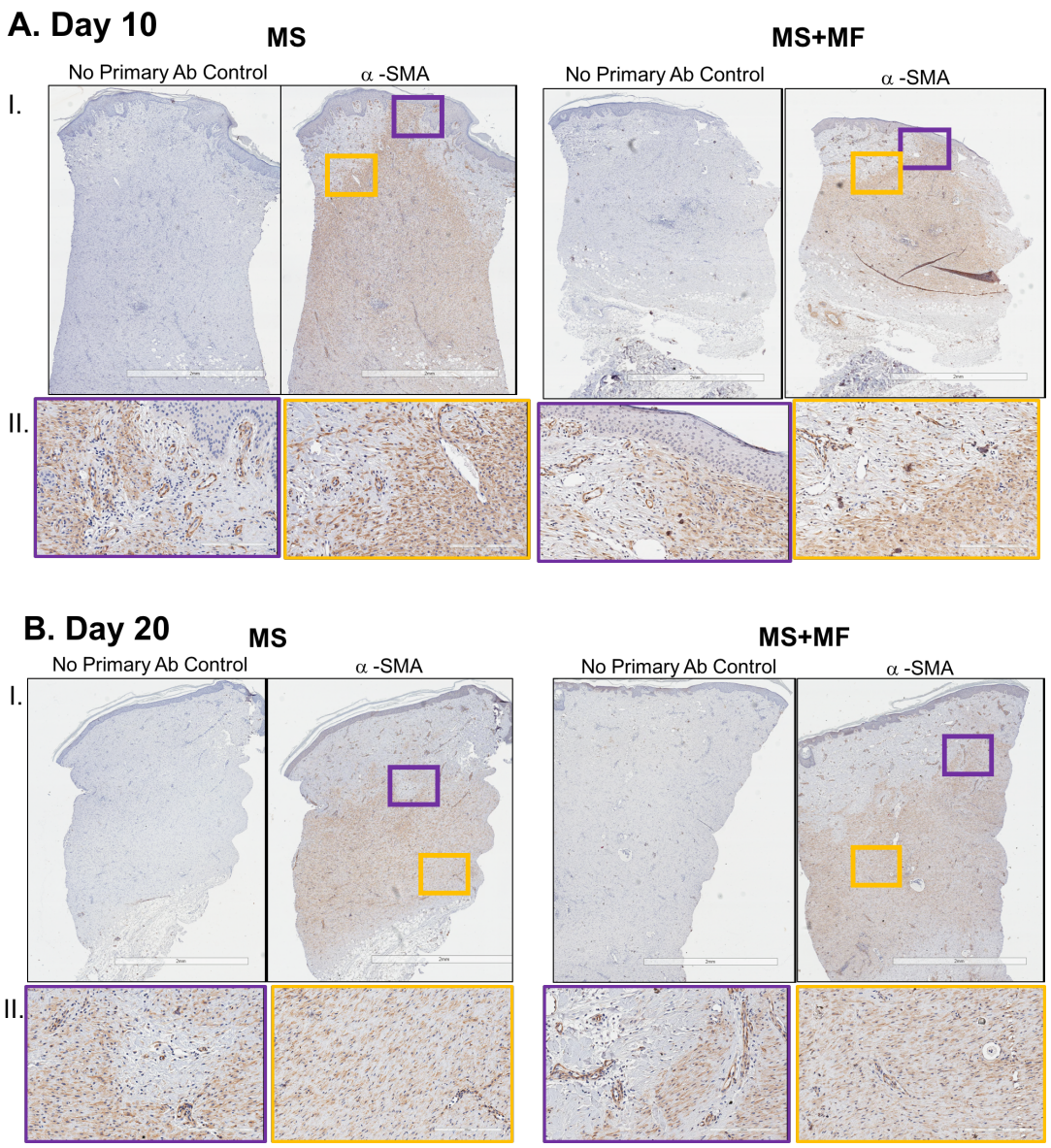


**Figure 3.6. Presence of dermal myofibroblasts on days 10 and 20 post-surgery** (**A,B**) **I.** Photomicrograph images showing α-SMA immunohistochemistry and no primary antibody (Ab) control in meshed skin (MS) and meshed skin + MeshFill (MS+MF) groups at 20x magnification. **II.** Corresponding color-coded magnifications at 200x showing α-SMA staining in the upper and lower dermis. Scale bars represent (**I.**) 2 mm and (**II.**) 200 μm (n=5-8).

### 3.3.7 Epidermal and dermal thickness

Hematoxylin and Eosin (H&E) stained tissue were examined to determine epidermal and dermal thickness of wounds. The data obtained were normalized to epidermal and dermal thickness of adjacent healthy skin. The epidermal thickness of MS+MF-treated wounds on day 60 showed no significant differences when compared to MS-treated wounds (97.32 ± 8.57 vs 107.10 ± 13.29 %). Similarly, no significant changes in dermal thickness were found (115.6 ± 8.60 vs 125.80 ± 10.17 %), but MS+MF treated wounds revealed an epidermal and dermal thickness that was more comparable to adjacent healthy skin.

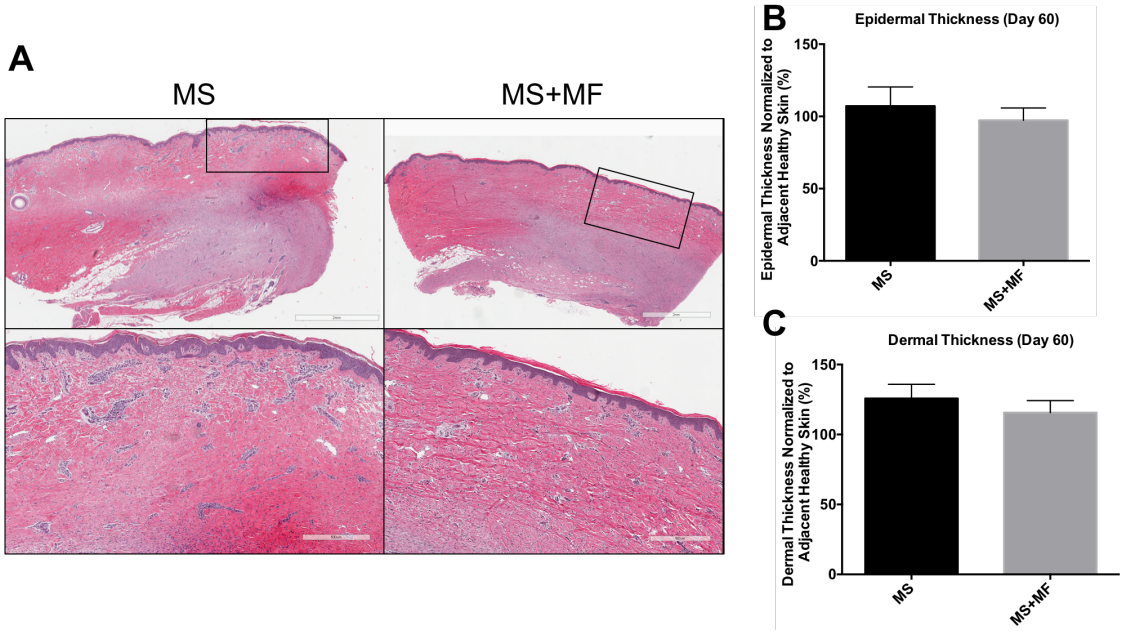


**Figure 3.7. Epidermal and dermal thickness 60 days post-surgery.** (**A**) Photomicrograph histology images showing epidermal and dermal thickness in meshed skin (MS) and meshed skin + MeshFill (MS+MF) groups. (**B**,**C**) Corresponding quantification of epidermal and dermal thickness at day 60 (n=5-8, $p > 0.05$). Scale bars represent 2 mm (upper panels) and 500 µm (lower panels).

### 3.4 Discussion

The advent of MSGs has saved lives of patients with burn injuries. Due to their ease of use and efficacy in treating full-thickness skin injuries, MSGs remain the current standard of care (75). However, despite these advantages, MSGs often lead to undesirable aesthetic outcomes. Although improvements in aesthetic outcomes have received attention by altering surgical techniques, this topic has not been examined closely in basic research (80, 112).

Due to healing by secondary intention in the fenestrated sites of MSGs, it is desirable to place a readily available biological liquid scaffold to fill the empty areas lacking a dermis. Studies examining the effects of skin substitutes when combined with MSGs are limited. One study conducted by the Apligraf® burn study group concluded that applying Apligraf® over MSGs in patients with burn injuries improved graft vascular perfusion, pliability, and cosmetic outcomes when compared to meshed skin control group (113). However, the lack of digital photographs and blinded evaluators was a limitation of this study.

Ideally, substances added to void areas of MSGs should take shape of the interstices and gelate *in-situ.* In this study, we added sufficient amount of MF to cover the void areas. As seen in figure 3.1 (A,B: I., II.), with 1.6 mL of hydrogel added (20% of the wound cavity), blinded evaluators judged the MS+MF group to be superior in cosmetic outcomes and reducing contractures. To provide further support for the above results, pliability of wounds should be examined in future studies.

A major concern in the use of skin grafts is secondary contractures, which can affect the functionality of the area that is grafted. The wound surface area was

examined on days 10, 20, and 60, and as seen in figure 3.2 (A,B), MS+MF group revealed a pattern of reduced contracture compared to MS alone, and this pattern persisted at all time points examined in this study. Although not significant, the patterns seen in figure 3.2 (A,B) provide support for the evaluators' scores of contracture (figure 3.1 B II.). Interestingly, the surface area of grafted wounds increased by day 60, but the overall surface area of MS+MF group remained relatively larger than the MS group. The expansion of scars with MSGs has been observed in previous studies using porcine animal models, and can be explained by the rapid growth of pigs from approximately 50 kg at day 20 to nearly 90 kg by day 60 (114, 115).

As a secondary objective, we examined wound healing outcomes using histological measures. Tissue cellularity (figure 3.3 A-D) and cell types (Figures 3.4-3.6) were identified in the wounds and scar areas. The results did not reveal significant differences in the tissue cellularity of wounds on days 10 and 20, but there was a marginal reduction in cellularity by day 60 in the MS+MF samples. It is plausible that the decreased cellularity can be due to the reduced number of myofibroblasts, leading to relatively reduced contractures seen in figure 3.2 (A,B). However, the results from this study do not provide support for that concept. As shown in figure 3.6 (A,B), there were no differences when α-SMA immunohistochemistry was examined qualitatively on days 10 and 20. However, as mentioned in the previous chapter, immunostaining and immunofluorescence intensity quantification of $\alpha$-SMA will provide a more reliable way to measure potential differences between MS+MF and MS groups at each time point.

With regards to the infiltration of T-lymphocytes and vessel-like structures in the dermis, similar outcomes of staining were observed as Chapter 2. Namely, the number

of vessel-like structures in the MS+MF groups were significantly reduced on day 10. Further, the number of T-lymphocytes (figure 3.5 A,B) showed a pattern of reduced $CD3^+$ T-cells in the MS+MF group on day 10 when compared to MS group. As expected, the number of vessel-like structures and T-lymphocytes continued to reduce in both groups by day 20, but there were no significant differences or patterns among the two groups at this time point. As explained in the previous chapter, the differences reported on day 10 may be due to the presence of MF accelerating the inflammatory phase and regression of blood vessels. However, due to the degradation of MF over time, these differences could have dissipated by day 20. Reapplication of MF after the dressing changes could potentially change these outcomes.

Finally, the epidermal and dermal thickness of MS and MS+MF samples were compared to adjacent healthy skin. As shown in figure 3.7 (A-C), both the epidermal and dermal thickness showed patterns in being more comparable to adjacent healthy skin in the MS+MF samples when compared to the MS samples. It is possible that with reapplication of MF, these differences could become more discernable and similar to healthy skin in the MS+MF samples.

In conclusion, this study has shown that the combination of MS and MF improved the cosmetic outcomes of fishnet-like scarring. Further, one-time application of MF reduced subjective evaluations of contractures in the MS+MF group. In order to gain further insights on the mechanisms leading to improved aesthetic outcomes and reduced contractures, experiments examining the pliability of wounds and expression of matrix remodeling proteins should be conducted. Moreover, for future studies, the Red Duroc pig may be a better animal model to use as this model is more prone to

contractures and hypertrophic scarring (116). Using the Red Duroc pig may lead to greater fishnet like scarring and potentially more prominent differences between MS+MF and MS groups. Nonetheless, the findings in this study have shown that an off-the-shelf, patient-ready hydrogel has the potential to be used in a clinical setting to improve aesthetic outcomes of scar formations in MSGs.

## Chapter 4: Discussion, limitations, and future directions

### 4.1 General Discussion

Burn injuries are devastating, leading to physical and psychological impacts on patients' health. Scars and hypertrophic scars resulting from these injuries cause functional and aesthetic complications (104). The use of skin grafts remains the gold-standard for large 3$^{rd}$ degree burn injuries, and its value cannot be underscored as this technology has saved lives of many patients. However, with advancements in tissue engineering, development of skin substitutes used in burn injuries trail behind. Many skin substitutes, whether in pre-clinical animal models or commercially available, have been shown to facilitate wound closure (117). But with burn injuries, functional and aesthetic outcomes are important factors to take into account. While functional recovery of skin grafts has progressed by surgical interventions, improvements in aesthetic outcomes of MSGs remain stagnant, ultimately leading to fishnet-like scar formation in patients (75).

The primary reason for scar formation is the lack of a dermis (118). Many products have attempted to emulate the dermal matrix components and properties (elasticity, integrity, and tensile strength). Integra™ dermal regeneration template is a pre-formed bi-layered construct comprised of bovine collagen and chondroitin-6-sulfate layer, and a superficial silicone layer (119). As mentioned previously, pre-formed constructs are limited in their adaptability to complex wound shapes. Integra™ also requires close surveillance to minimize the occurrence of infections under the silicone layer before its removal. Further, though it is an off-the-shelf skin substitute, the high cost associated with this product makes it unfeasible for routine clinical use. Matriderm®

is another commercially available skin substitute composed of a collagen-elastin matrix, and when compared to Integra™ in full-thickness wounds of rats, no major differences in healing rates were found (120, 121). Indeed, a study by Philandrianos group compared five dermal substitutes (Integra™, Renoskin®, Matriderm®, Proderm®, Hyalomatrix®) in a full-thickness porcine model, and concluded that the use of these skin substitute, followed by split-thickness meshed skin grafting after 3 weeks made no difference in the long-term (6 months) scar quality of wounds (115). Thus, due to the lack of consistency in healing outcomes of deep wounds using various commercially available skin substitutes, the need for a reliable, off-the-shelf, and cost-effective skin substitute that improves aesthetic outcomes in burn injuries is crucial.

Previously, our group showed that MF gelates *in-situ* in approximately 15 minutes, and the application of MF in full-thickness wounds in a rabbit ear model reduced scar elevation index, in addition to wound healing outcomes assessed through histology and immunofluorescence staining (92). In the pilot study presented in this thesis, we assessed the wound healing outcomes through a one-time application of MF in full-thickness wounds, and in combination with split-thickness MSGs. In Chapter 2, we showed that wounds without MF contracted significantly more on day 20 compared to MF-treated group. In the third chapter, results of blinded evaluations showed that the combination of MS and MF (MS+MF) were evaluated to have significantly better aesthetic outcomes compared to MS alone. Further, blinded assessments showed that MS+MF group was perceived to be significantly less contracted compared to MS group on day 60. When contracture was quantified through wound area analysis, only patterns of MS+MF group being less contracted compared to MS group was reported. These

results aligned with previous *in-vitro* work done by our group showing the resistance of MF to HSc fibroblasts when compared to a standard collagen:GAG matrix (91).

### 4.2 Limitations and Future Directions

In this pilot study, we utilized Yorkshire pigs as an animal model to examine the healing of MSGs as this breed of pigs closely resembled the healing of full-thickness wounds in healthy human skin (122). When wounds from groups with MSGs were compared, we observed that the extent of fishnet-like scarring present in Yorkshire pigs was comparatively less than those seen in humans with MSGs meshed at a 3:1 ratio. This may be due to the use of excisional wounds rather burn wound in this study. Unlike excisional injuries, burn injuries have varying thicknesses, and a different biochemical milieu that cannot be replicated in excisional wounds (123). Indeed, when compared to excisional wounds in Red Duroc pigs, a previous study found that burn scars healed at a slower rate, contracted more, and were less pliable, elastic, and weaker when compared with excisional wounds (123). As a result, future studies using a burn-excision model may be more suitable to enhance the scar profiles of wounds with MSGs (124).

If limitations in equipment prohibit the use of a burn-excision model, larger expansion ratios (6:1) are recommended to show discernable differences in fishnet-like scar formation, and potentially reveal more robust differences in the aesthetic outcomes of MF-treated MSGs when compared to MSGs alone.

Moreover, in order to improve the clinical feasibility and user-friendly status of MF in deep wounds, an increase in viscosity and reduced gelation time of scaffold is

suggested. Though MF can be useful for tunneled wounds, such as pressure ulcers, the liquid state of MF is not ideal for large wounds, as this state allows escaping of the liquid scaffold from the site of injury. Thus, the addition of inert agents, such as guar gum or alginates should be examined to assess viscosity of MF pre-gelation, and its ability to form a honey-like substance that can easily be added to fill void areas of MSGs without compromising cell adherence and morphology within the scaffold (125). Alternatively, it would be interesting for future studies to examine the mechanism by which PVA-PEG interact with collagen to improve gelation time while providing a more viscous scaffold.

As contractures present a major issue with functional and aesthetic outcomes of MSGs, it would be useful to investigate incorporating elastin into our hydrogel formulation. In healthy skin, elastin serves to maintain the structural and mechanical integrity of skin, in addition to playing a role in cell signaling (126). Previous studies have shown reduced fibroblast differentiation into myofibroblasts, and increased dedifferentiation of myofibroblasts with increasing matrix elasticity (127, 128). Further, collagen-elastin scaffolds have been shown to promote synthesis of elastic fibers (129). Thus, incorporating elastin into MF may decrease secondary wound contractures and improve aesthetic outcomes. A concern in elastin-containing scaffolds is the extreme insolubility of elastin, but with the advent of recombinant forms of human tropoelastin and elastin-like peptides, solubility and incorporation into skin substitute matrices is greatly facilitated (126, 130).

A common finding in commercially available skin substitutes is a foreign body reaction (115). In our study, we observed the presence of foreign body giant cells in MF-treated groups (data not shown), but to our knowledge, this did not interfere with wound

healing outcomes. Future studies will examine the role of giant cells in MF-treated wounds, and examine ways to attenuate this response. One plausible reason for the presence of giant cells is due to glutaraldehyde, a collagen chemical cross-linker used in the formulation of MF (131). To minimize a foreign body reaction, the use of alternative cross-linkers should be explored.

## Bibliography

1. Gantwerker EA, Hom DB. Skin: histology and physiology of wound healing. Facial Plast Surg Clin North Am. 2011;19(3):441-53.

2. Burns T, Breathnach, S., Cox, N., & Griffiths, C. Anatomy and Organization of Human Skin. Rook's Textbook of Dermatology 2010.

3. Menon GK, Cleary GW, Lane ME. The structure and function of the stratum corneum. Int J Pharm. 2012;435(1):3-9.

4. Kamolz L-P, Jeschke MG, Herndon DN, Horch RE, Brychta P, Küntscher M, et al. Handbook of Burns Volume 2: Reconstruction and Rehabilitation. 1. Aufl.;1st; ed. New York: Springer; 2011.

5. Zhang Z, Ortiz O, Goyal R, Kohn J. Chapter 23 - Biodegradable Polymers A2 - Lanza, Robert. In: Langer R, Vacanti J, editors. Principles of Tissue Engineering (Fourth Edition). Boston: Academic Press; 2014. p. 441-73.

6. Riekki R, Parikka M, Jukkola A, Salo T, Risteli J, Oikarinen A. Increased expression of collagen types I and III in human skin as a consequence of radiotherapy. Archives of Dermatological Research. 2002;294(4):178-84.

7. Ricard-Blum S. The collagen family. Cold Spring Harb Perspect Biol. 2011;3(1):a004978.

8. Thakur R, Batheja P, Kaushik D, Michniak B. Chapter 4 - Structural and Biochemical Changes in Aging Skin and Their Impact on Skin Permeability Barrier. In: Dayan N, editor. Skin Aging Handbook. Norwich, NY: William Andrew Publishing; 2009. p. 55-90.

9. Singer AJ, Clark RA. Cutaneous wound healing. N Engl J Med. 1999;341(10):738-46.

10. Zomer HD, Trentin AG. Skin wound healing in humans and mice: Challenges in translational research. J Dermatol Sci. 2018;90(1):3-12.

11. Eming SA, Martin P, Tomic-Canic M. Wound repair and regeneration: mechanisms, signaling, and translation. Sci Transl Med. 2014;6(265):265sr6.

12. Diegelmann RF, Evans MC. Wound healing: an overview of acute, fibrotic and delayed healing. Front Biosci. 2004;9:283-9.

13. Dovi JV, Szpaderska AM, DiPietro LA. Neutrophil function in the healing wound: adding insult to injury? Thromb Haemost. 2004;92(2):275-80.

14. Landen NX, Li D, Stahle M. Transition from inflammation to proliferation: a critical step during wound healing. Cell Mol Life Sci. 2016;73(20):3861-85.

15. Mosser DM. The many faces of macrophage activation. J Leukoc Biol. 2003;73(2):209-12.

16. Barrientos S, Stojadinovic O, Golinko MS, Brem H, Tomic-Canic M. Growth factors and cytokines in wound healing. Wound Repair Regen. 2008;16(5):585-601.

17. Galli SJ, Borregaard N, Wynn TA. Phenotypic and functional plasticity of cells of innate immunity: macrophages, mast cells and neutrophils. Nat Immunol. 2011;12(11):1035-44.

18. DiPietro LA. Wound healing: the role of the macrophage and other immune cells. Shock. 1995;4(4):233-40.

19. Greenlee-Wacker MC. Clearance of apoptotic neutrophils and resolution of inflammation. Immunol Rev. 2016;273(1):357-70.

20. Hesketh M, Sahin KB, West ZE, Murray RZ. Macrophage Phenotypes Regulate Scar Formation and Chronic Wound Healing. Int J Mol Sci. 2017;18(7).

21. Laurens N, Koolwijk P, de Maat MP. Fibrin structure and wound healing. J Thromb Haemost. 2006;4(5):932-9.

22. Semenza GL. Vasculogenesis, angiogenesis, and arteriogenesis: mechanisms of blood vessel formation and remodeling. J Cell Biochem. 2007;102(4):840-7.

23. Michiels C, Arnould T, Remacle J. Hypoxia-induced activation of endothelial cells as a possible cause of venous diseases: hypothesis. Angiology. 1993;44(8):639-46.

24. Li J, Zhang YP, Kirsner RS. Angiogenesis in wound repair: angiogenic growth factors and the extracellular matrix. Microsc Res Tech. 2003;60(1):107-14.

25. Nagy JA, Benjamin L, Zeng H, Dvorak AM, Dvorak HF. Vascular permeability, vascular hyperpermeability and angiogenesis. Angiogenesis. 2008;11(2):109-19.

26. Murakami M, Simons M. Fibroblast growth factor regulation of neovascularization. Curr Opin Hematol. 2008;15(3):215-20.

27. Saunders WB, Bohnsack BL, Faske JB, Anthis NJ, Bayless KJ, Hirschi KK, et al. Coregulation of vascular tube stabilization by endothelial cell TIMP-2 and pericyte TIMP-3. J Cell Biol. 2006;175(1):179-91.

28. Nguyen M, Arkell J, Jackson CJ. Human endothelial gelatinases and angiogenesis. Int J Biochem Cell Biol. 2001;33(10):960-70.

29. Heng MC. Wound healing in adult skin: aiming for perfect regeneration. Int J Dermatol. 2011;50(9):1058-66.

30. Pastar I, Stojadinovic O, Yin NC, Ramirez H, Nusbaum AG, Sawaya A, et al. Epithelialization in Wound Healing: A Comprehensive Review. Adv Wound Care (New Rochelle). 2014;3(7):445-64.

31. Li B, Wang JH. Fibroblasts and myofibroblasts in wound healing: force generation and measurement. J Tissue Viability. 2011;20(4):108-20.

32. Levenson SM, Geever EF, Crowley LV, Oates JF, 3rd, Berard CW, Rosen H. The Healing of Rat Skin Wounds. Ann Surg. 1965;161:293-308.

33. Wietecha MS, Cerny WL, DiPietro LA. Mechanisms of vessel regression: toward an understanding of the resolution of angiogenesis. Curr Top Microbiol Immunol. 2013;367:3-32.

34. Gantwerker EA, Hom DB. Skin: histology and physiology of wound healing. Clin Plast Surg. 2012;39(1):85-97.

35. Bailey AJ, Sims TJ, Le L, bazin S. Collagen polymorphism in experimental granulation tissue. Biochem Biophys Res Commun. 1975;66(4):1160-5.

36. Robins SP, Milne G, Duncan A, Davies C, Butt R, Greiling D, et al. Increased skin collagen extractability and proportions of collagen type III are not normalized after 6 months healing of human excisional wounds. The Journal of investigative dermatology. 2003;121(2):267-72.

37. Gelse K, Poschl E, Aigner T. Collagens--structure, function, and biosynthesis. Adv Drug Deliv Rev. 2003;55(12):1531-46.

38. Asgari M, Latifi N, Heris HK, Vali H, Mongeau L. In vitro fibrillogenesis of tropocollagen type III in collagen type I affects its relative fibrillar topology and mechanics. Sci Rep. 2017;7(1):1392.

39. Darby IA, Laverdet B, Bonte F, Desmouliere A. Fibroblasts and myofibroblasts in wound healing. Clin Cosmet Investig Dermatol. 2014;7:301-11.

40. Xue M, Jackson CJ. Extracellular Matrix Reorganization During Wound Healing and Its Impact on Abnormal Scarring. Adv Wound Care (New Rochelle). 2015;4(3):119-36.

41. Peck M, Molnar J, Swart D. A global plan for burn prevention and care. Bull World Health Organ. 2009;87(10):802-3.

42. Atiyeh BS, Gunn SW, Hayek SN. State of the art in burn treatment. World J Surg. 2005;29(2):131-48.

43. Atiyeh BS, Hayek SN, Gunn SW. New technologies for burn wound closure and healing--review of the literature. Burns. 2005;31(8):944-56.

44. Goel A, Shrivastava P. Post-burn scars and scar contractures. Indian J Plast Surg. 2010;43(Suppl):S63-71.

45. Cumming J, Purdue GF, Hunt JL, O'Keefe GE. Objective estimates of the incidence and consequences of multiple organ dysfunction and sepsis after burn trauma. J Trauma. 2001;50(3):510-5.

46. Hettiaratchy S, Dziewulski P. ABC of burns: pathophysiology and types of burns. BMJ. 2004;328(7453):1427-9.

47. Valencia IC, Falabella AF, Eaglstein WH. SKIN GRAFTING. Dermatologic Clinics.18(3):521-32.

48. Ratner D. Skin grafting. Semin Cutan Med Surg. 2003;22(4):295-305.

49. Boudana D, Wolber A, Coeugniet E, Martinot-Duquennoy V, Pellerin P. [History of skin graft]. Ann Chir Plast Esthet. 2010;55(4):328-32.

50. Tanner JJC, Vandeput J, Olley JF. THE MESH SKIN GRAFT. Plastic and reconstructive surgery. 1964;34(3):287-92.

51. Shimizu R, Kishi K. Skin graft. Plast Surg Int. 2012;2012:563493.

52. Moran SL, Sems SA, Ovid Technologies I. Soft tissue surgery. 2nd ed. Philadelphia: Wolters Kluwer; 2017.

53. Complications Involved in Various Surgical Techniques. In: Gupta DK, editor. Microskin Grafting for Vitiligo. London: Springer London; 2009. p. 119-24.

54. Kubota Y, Mitsukawa N, Chuma K, Akita S, Sasahara Y, Rikihisa N, et al. Hyperpigmentation after surgery for a deep dermal burn of the dorsum of the hand: partial-thickness debridement followed by medium split-thickness skin grafting vs full-thickness debridement followed by thick split-thickness skin grafting. Burns Trauma. 2016;4:9.

55. Rohrer TE, Cook JL, Kaufman AJ. Flaps and grafts in dermatologic surgery. 2018.

56. Converse JM, Uhlschmid GK, Ballantyne DL, Jr. "Plasmatic circulation" in skin grafts. The phase of serum imbibition. Plast Reconstr Surg. 1969;43(5):495-9.

57. Psillakis JM, de Jorge FB, Villardo R, de Albano AM, Martins M, Spina V. Water and electrolyte changes in autogenous skin grafts. Discussion of the so-called "plasmatic circulation". Plast Reconstr Surg. 1969;43(5):500-3.

58. Laschke MW, Menger MD. Vascularization in tissue engineering: angiogenesis versus inosculation. Eur Surg Res. 2012;48(2):85-92.

59. Smahel J. The revascularization of a free skin autograft. Acta Chir Plast. 1967;9(1):76-7.

60. Okada T. Revascularisation of free full thickness skin grafts in rabbits: a scanning electron microscope study of microvascular casts. British Journal of Plastic Surgery.39(2):183-9.

61. Young DM, Greulich KM, Weier HG. Species-specific in situ hybridization with fluorochrome-labeled DNA probes to study vascularization of human skin grafts on athymic mice. J Burn Care Rehabil. 1996;17(4):305-10.

62. Marckmann A. Autologous skin grafts in the rat: vital microscopic studies of the microcirculation. Angiology. 1966;17(7):475-82.

63. Clemmesen T. (the Early Circulation in Split-Skin Grafts. Restoration of Blood Supply to Split-Skin Autografts.). Acta Chir Scand. 1964;127:1-8.

64. Birch J, Branemark PI. The vascularization of a free full thickness skin graft. I. A vital microscopic study. Scand J Plast Reconstr Surg. 1969;3(1):1-10.

65. Birch J, Branemark PI, Nilsson K. The vascularization of a free full thickness skin graft. 3. An infrared thermographic study. Scand J Plast Reconstr Surg. 1969;3(1):18-22.

66. Medawar PB. The behaviour and fate of skin autografts and skin homografts in rabbits: A report to the War Wounds Committee of the Medical Research Council. J Anat. 1944;78(Pt 5):176-99.

67. Birch J, Branemark PI, Lundskog J. The vascularization of a free full thickness skin graft. II. A microangiographic study. Scand J Plast Reconstr Surg. 1969;3(1):11-7.

68. Zarem HA. Development of the microcirculation in full thickness autogenous skin grafts in mice. Surg Forum. 1965;16:469-70.

69. Converse JM, Ballantyne DL, Jr. Distribution of diphosphopyridine nucleotide diaphorase in rat skin autografts and homografts. Plast Reconstr Surg Transplant Bull. 1962;30:415-25.

70. Goretsky MJ, Breeden M, Pisarski G, Harriger MD, Boyce ST, Greenhalgh DG. Capillary morphogenesis during healing of full-thickness skin grafts: an ultrastructural study. Wound Repair Regen. 1995;3(2):213-20.

71. Capla JM, Ceradini DJ, Tepper OM, Callaghan MJ, Bhatt KA, Galiano RD, et al. Skin graft vascularization involves precisely regulated regression and replacement of endothelial cells through both angiogenesis and vasculogenesis. Plast Reconstr Surg. 2006;117(3):836-44.

72. O'Ceallaigh S, Herrick SE, Bluff JE, McGrouther DA, Ferguson MW. Quantification of total and perfused blood vessels in murine skin autografts using a fluorescent double-labeling technique. Plast Reconstr Surg. 2006;117(1):140-51.

73. Hong G, Lee JC, Robinson JT, Raaz U, Xie L, Huang NF, et al. Multifunctional in vivo vascular imaging using near-infrared II fluorescence. Nat Med. 2012;18(12):1841-6.

74. Jeschke MG, Shahrokhi S, Finnerty CC, Branski LK, Dibildox M, Organization ABA, et al. Wound Coverage Technologies in Burn Care: Established Techniques. J Burn Care Res. 2018.

75. Singh M, Nuutila K, Collins KC, Huang A. Evolution of skin grafting for treatment of burns: Reverdin pinch grafting to Tanner mesh grafting and beyond. Burns. 2017;43(6):1149-54.

76. Pripotnev S, Papp A. Split thickness skin graft meshing ratio indications and common practices. Burns. 2017;43(8):1775-81.

77. Farroha A, Frew Q, El-Muttardi N, Philp B, Dziewulski P. The use of Biobrane(R) to dress split-thickness skin graft in paediatric burns. Ann Burns Fire Disasters. 2013;26(2):94-7.

78. Pope ER. Mesh skin grafting. Vet Clin North Am Small Anim Pract. 1990;20(1):177-87.

79. Bern R, Serror K, Alvo R, Chaouat M, Mimoun M, Schmidt M, et al. Original and modified technique of tie-over dressing: Method and application in burn patients. Burns. 2018.

80. Hazani R, Whitney R, Wilhelmi BJ. Optimizing aesthetic results in skin grafting. Am Surg. 2012;78(2):151-4.

81. Fang RC, Mustoe TA. Animal models of wound healing: utility in transgenic mice. J Biomater Sci Polym Ed. 2008;19(8):989-1005.

82. Abdullahi A, Amini-Nik S, Jeschke MG. Animal models in burn research. Cell Mol Life Sci. 2014;71(17):3241-55.

83. Davidson JM, Yu F, Opalenik SR. Splinting Strategies to Overcome Confounding Wound Contraction in Experimental Animal Models. Adv Wound Care (New Rochelle). 2013;2(4):142-8.

84. Gerber PA, Buhren BA, Schrumpf H, Homey B, Zlotnik A, Hevezi P. The top skin-associated genes: a comparative analysis of human and mouse skin transcriptomes. Biol Chem. 2014;395(6):577-91.

85. Sullivan TP, Eaglstein WH, Davis SC, Mertz P. The pig as a model for human wound healing. Wound Repair Regen. 2001;9(2):66-76.

86. Seaton M, Hocking A, Gibran NS. Porcine models of cutaneous wound healing. ILAR J. 2015;56(1):127-38.

87. Tiwari VK. Burn wound: How it differs from other wounds? Indian J Plast Surg. 2012;45(2):364-73.

88. Greenwood JE, Clausen J, Kavanagh S. Experience with biobrane: uses and caveats for success. Eplasty. 2009;9:e25.

89. Field FK, Kerstein MD. Overview of wound healing in a moist environment. Am J Surg. 1994;167(1A):2S-6S.

90. Hartwell R, Chan B, Elliott K, Alnojeidi H, Ghahary A. Polyvinyl alcohol-graft-polyethylene glycol hydrogels improve utility and biofunctionality of injectable collagen biomaterials. Biomed Mater. 2016;11(3):035013.

91. Hartwell R, Leung V, Chavez-Munoz C, Nabai L, Yang H, Ko F, et al. A novel hydrogel-collagen composite improves functionality of an injectable extracellular matrix. Acta Biomater. 2011;7(8):3060-9.

92. Hartwell R, Poormasjedi-Meibod MS, Chavez-Munoz C, Jalili RB, Hosseini-Tabatabaei A, Ghahary A. An in-situ forming skin substitute improves healing outcome in a hypertrophic scar model. Tissue Eng Part A. 2015;21(5-6):1085-94.

93. Varkey M, Ding J, Tredget EE. Advances in Skin Substitutes-Potential of Tissue Engineered Skin for Facilitating Anti-Fibrotic Healing. J Funct Biomater. 2015;6(3):547-63.

94. Brem H, Stojadinovic O, Diegelmann RF, Entero H, Lee B, Pastar I, et al. Molecular markers in patients with chronic wounds to guide surgical debridement. Mol Med. 2007;13(1-2):30-9.

95. Hop MJ, Polinder S, van der Vlies CH, Middelkoop E, van Baar ME. Costs of burn care: a systematic review. Wound Repair Regen. 2014;22(4):436-50.

96. Supp DM, Boyce ST. Engineered skin substitutes: practices and potentials. Clin Dermatol. 2005;23(4):403-12.

97. Burd A, Chiu T. Allogenic skin in the treatment of burns. Clin Dermatol. 2005;23(4):376-87.

98. Augustine R, Kalarikkal N, Thomas S. Advancement of wound care from grafts to bioengineered smart skin substitutes. Prog Biomater. 2014;3(2-4):103-13.

99. MacNeil S. Progress and opportunities for tissue-engineered skin. Nature. 2007;445(7130):874-80.

100. Spang MT, Christman KL. Extracellular matrix hydrogel therapies: In vivo applications and development. Acta Biomater. 2018;68:1-14.

101. Akhtar MF, Hanif M, Ranjha NM. Methods of synthesis of hydrogels ... A review. Saudi Pharm J. 2016;24(5):554-9.

102. Rahmani Del Bakhshayesh A, Annabi N, Khalilov R, Akbarzadeh A, Samiei M, Alizadeh E, et al. Recent advances on biomedical applications of scaffolds in wound healing and dermal tissue engineering. Artif Cells Nanomed Biotechnol. 2018;46(4):691-705.

103. Li M, Moeen Rezakhanlou A, Chavez-Munoz C, Lai A, Ghahary A. Keratinocyte-releasable factors increased the expression of MMP1 and MMP3 in co-cultured fibroblasts under both 2D and 3D culture conditions. Mol Cell Biochem. 2009;332(1-2):1-8.

104. Jeschke MG, Finnerty CC, Shahrokhi S, Branski LK, Dibildox M, Organization ABA, et al. Wound coverage technologies in burn care: novel techniques. J Burn Care Res. 2013;34(6):612-20.

105. Junker JP, Kamel RA, Caterson EJ, Eriksson E. Clinical Impact Upon Wound Healing and Inflammation in Moist, Wet, and Dry Environments. Adv Wound Care (New Rochelle). 2013;2(7):348-56.

106. Rettinger CL, Fletcher JL, Carlsson AH, Chan RK. Accelerated epithelialization and improved wound healing metrics in porcine full-thickness wounds transplanted with full-thickness skin micrografts. Wound Repair Regen. 2017;25(5):816-27.

107. Sirousazar M, Yari M. Dehydration kinetics of polyvinyl alcohol hydrogel wound dressings during wound healing process. Chinese Journal of Polymer Science. 2010;28(4):573-80.

108. Jain M, Khadilkar N, De Sousa A. Burn-related factors affecting anxiety, depression and self-esteem in burn patients: an exploratory study. Ann Burns Fire Disasters. 2017;30(1):30-4.

109. Abdullah A, Blakeney P, Hunt R, Broemeling L, Phillips L, Herndon DN, et al. Visible scars and self-esteem in pediatric patients with burns. J Burn Care Rehabil. 1994;15(2):164-8.

110. Reid MJ, Currie LJ, James SE, Sharpe JR. Effect of artificial dermal substitute, cultured keratinocytes and split thickness skin graft on wound contraction. Wound Repair Regen. 2007;15(6):889-96.

111. Sakamoto M, Morimoto N, Inoie M, Takahagi M, Ogino S, Jinno C, et al. Cultured Human Epidermis Combined With Meshed Skin Autografts Accelerates Epithelialization and Granulation Tissue Formation in a Rat Model. Ann Plast Surg. 2017;78(6):651-8.

112. Sajad W, Hamid R. Outcome of split thickness skin grafting and multiple z-plasties in postburn contractures of groin and perineum: a 15-year experience. Plast Surg Int. 2014;2014:358526.

113. Waymack P, Duff RG, Sabolinski M. The effect of a tissue engineered bilayered living skin analog, over meshed split-thickness autografts on the healing of excised burn wounds. The Apligraf Burn Study Group. Burns. 2000;26(7):609-19.

114. Fifer TD, Pieper D, Hawtof D. Contraction rates of meshed, nonexpanded split-thickness skin grafts versus split-thickness sheet grafts. Ann Plast Surg. 1993;31(2):162-3.

115. Philandrianos C, Andrac-Meyer L, Mordon S, Feuerstein JM, Sabatier F, Veran J, et al. Comparison of five dermal substitutes in full-thickness skin wound healing in a porcine model. Burns. 2012;38(6):820-9.

116. Zhu KQ, Carrougher GJ, Gibran NS, Isik FF, Engrav LH. Review of the female Duroc/Yorkshire pig model of human fibroproliferative scarring. Wound Repair Regen. 2007;15 Suppl 1:S32-9.

117. Halim AS, Khoo TL, Mohd Yussof SJ. Biologic and synthetic skin substitutes: An overview. Indian J Plast Surg. 2010;43(Suppl):S23-8.

118. Evans ND, Oreffo RO, Healy E, Thurner PJ, Man YH. Epithelial mechanobiology, skin wound healing, and the stem cell niche. J Mech Behav Biomed Mater. 2013;28:397-409.

119. Dantzer E, Braye FM. Reconstructive surgery using an artificial dermis (Integra): results with 39 grafts. Br J Plast Surg. 2001;54(8):659-64.

120. Schneider J, Biedermann T, Widmer D, Montano I, Meuli M, Reichmann E, et al. Matriderm versus Integra: a comparative experimental study. Burns. 2009;35(1):51-7.

121. Bottcher-Haberzeth S, Biedermann T, Schiestl C, Hartmann-Fritsch F, Schneider J, Reichmann E, et al. Matriderm(R) 1 mm versus Integra(R) Single Layer 1.3 mm for one-step closure of full thickness skin defects: a comparative experimental study in rats. Pediatr Surg Int. 2012;28(2):171-7.

122. Gallant-Behm CL, Tsao H, Reno C, Olson ME, Hart DA. Skin wound healing in the first generation (F1) offspring of Yorkshire and red Duroc pigs: evidence for genetic inheritance of wound phenotype. Burns. 2006;32(2):180-93.

123. Blackstone BN, Kim JY, McFarland KL, Sen CK, Supp DM, Bailey JK, et al. Scar formation following excisional and burn injuries in a red Duroc pig model. Wound Repair Regen. 2017;25(4):618-31.

124. Singer AJ, Toussaint J, Chung WT, McClain SA, Raut V, Rosenberg L. Early versus Delayed Excision and Grafting of Full-Thickness Burns in a Porcine Model: A Randomized Study. Plast Reconstr Surg. 2016;137(6):972e-9e.

125. Sun J, Tan H. Alginate-Based Biomaterials for Regenerative Medicine Applications. Materials (Basel). 2013;6(4):1285-309.

126. Rnjak J, Wise SG, Mithieux SM, Weiss AS. Severe burn injuries and the role of elastin in the design of dermal substitutes. Tissue Eng Part B Rev. 2011;17(2):81-91.

127. Kloxin AM, Benton JA, Anseth KS. In situ elasticity modulation with dynamic substrates to direct cell phenotype. Biomaterials. 2010;31(1):1-8.

128. Meyer-ter-Vehn T, Han H, Grehn F, Schlunck G. Extracellular matrix elasticity modulates TGF-beta-induced p38 activation and myofibroblast transdifferentiation in human tenon fibroblasts. Invest Ophthalmol Vis Sci. 2011;52(12):9149-55.

129. Daamen WF, Nillesen ST, Wismans RG, Reinhardt DP, Hafmans T, Veerkamp JH, et al. A biomaterial composed of collagen and solubilized elastin enhances angiogenesis and elastic fiber formation without calcification. Tissue Eng Part A. 2008;14(3):349-60.

130. Zhang YN, Avery RK, Vallmajo-Martin Q, Assmann A, Vegh A, Memic A, et al. A Highly Elastic and Rapidly Crosslinkable Elastin-Like Polypeptide-Based Hydrogel for Biomedical Applications. Adv Funct Mater. 2015;25(30):4814-26.

131. Yu T, Wang W, Nassiri S, Kwan T, Dang C, Liu W, et al. Temporal and spatial distribution of macrophage phenotype markers in the foreign body response to glutaraldehyde-crosslinked gelatin hydrogels. J Biomater Sci Polym Ed. 2016;27(8):721-42.